Numerical Approach to the Dynamics of Quantum Gravity

(量子重力のダイナミクスに対する数値的アプローチ)

西　村　　淳

学 位 論 文

Numerical Approach to the Dynamics of Quantum Gravity

(量子重力のダイナミクスに対する数値的アプローチ)

平成7年3月博士(理学)申請

東京大学大学院理学系研究科

物理学専攻

西 村 淳

Numerical Approach to the Dynamics of Quantum Gravity

Ph. D. Thesis

JUN NISHIMURA*

Department of Physics, University of Tokyo,
Bunkyo-ku, Tokyo 113, Japan

*E-mail address : nishi@danjuro.phys.s.u-tokyo.ac.jp, JSPS Research Fellow.

Abstract

There are two methods currently used as a lattice regularization of quantum gravity, namely dynamical triangulation and Regge calculus. Although dynamical triangulation can be naturally expected to be a proper regularization of quantum gravity, Regge calculus does not have any grounds of restoring the general covariance in the continuum limit. We study fractal structure in two-dimensional quantum Regge calculus and show that the expected loop–length distribution is reproduced for the type of loops that is attached to baby universes, when the scale–invariant measure is adopted. This suggests the possibility that Regge calculus might restore the general covariance in the continuum limit if the measure of the link–length integration is properly chosen.

We next present our results of numerical simulation of four–dimensional quantum gravity based on dynamical triangulation. Although it has been known for some time that there is a second–order phase transition, it is still unclear whether we can take a sensible continuum limit at the critical point. We measure vertex–order distribution and show that, in the strong–coupling phase, there is a vertex with very large order. We then put in the action an additional term which suppresses the vertex with very large order, and observe that the system is always in the branched–polymer phase. We also present a clue that the branched–polymer structure is related to the conformal–mode instability.

Contents

Chapter 1

Introduction

1.1 Motivations of quantum gravity

Although gravity has been known to people since Newton's theory, it is the only force that is not understood within quantum theory. Actually, gravitational interaction between elementary particles is negligibly small compared with the other forces unless we look at phenomena with energy higher than the Planck scale (10^{19}GeV). It is because this energy scale is too far above the energy scale within the reach of the present experiments that the Standard Model works very well without gravity. In fact the Planck scale is even much higher than the energy scale that human beings can achieve in future through collider experiments. One might, therefore, ask why we should study quantum gravity, for we will never see it.

On the other hand, we all know that the Standard Model contains a lot of free parameters such as particle masses and coupling constants that have to be put in by hand. We cannot also answer why the gauge group is $SU(3) \times SU(2) \times U(1)$ or why the space–time dimension is four. It is natural for us to hope that the key to all these mysteries lies in higher energy scale. Recent data of precise measurement of the gauge coupling constants strongly suggest that the three forces are unified into

a Grand Unified Theory at about 10^{16}GeV. We should say that this energy scale is quite near the Planck scale, which gives us a hope that all the four forces including gravity are unified around this energy scale. From this point of view, all the details of the Standard Model are the experimental facts which should be explained as the low–energy effective theory of the fundamental theory, which inevitably includes the quantum effects of gravity.

The special aspect of gravity which makes it different from the other forces is that it is described by the dynamics of the space–time as is discovered by Einstein. It is nothing but this fact that makes the quantum theory of gravitation not only exciting but also difficult. Planck scale physics is not a dream of high energy physicists, but a reality which must certainly have played a crucial role at the very beginning of the universe. At the same time, there are a lot of conceptual problems concerning the physical interpretation. First of all, one may worry about probabilistic interpretation of quantum gravity, when time itself is included in the dynamical variables. It is also problematic whether we can interpret the wave function of the universe by separating the whole thing into the observer and the system to be observed. Furthermore, we may have to give up the description of the theory in terms of time evolution and be contented with reproducing our conventional picture in the classical limit. We think, therefore, that we should try to solve the dynamics of quantum gravity first instead of being too speculative about these conceptual problems.

There are two formulations with which we can treat quantum gravity. One is the string theory and the other is an ordinary field theory. Although string theory is attractive, since it is the only candidate for "Theory of Everything" at present, it turned out that the non–perturbative formulation is necessary in order to make any physical prediction. On the other hand, exploring the ordinary field–theoretical approach to quantum gravity is important for its own sake, since it describes the fluctuation of the space–time geometry, which is necessary in studying black–hole physics or quantum cosmology at early universe, even if string theory is successfully solved. The field–theoretical approach will also give us information on string theory. If it turns out that higher–dimensional quantum gravity can be formulated, then it

provides us with a constraint on string theory, since it has to be reproduced as an effective theory of string theory in the point–particle limit. If the answer turns out to be negative, then we should be keener on string theory, not only because it is the only consistent theory that can describe quantum gravity but also because it is the only consistent theory of extended objects.

Apart from these motivations of quantum gravity, we would like to emphasize that quantum gravity is related to various branches of physics such as theories of membrane, non–perturbative effects of gauge theories, and so on. When we look back on the history of particle physics, we find that crucial steps in understanding the Nature have always been brought about through a new insight into the dynamics of field theories. For example, the discovery of spontaneous symmetry breakdown and the Higgs mechanism were essential to the establishment of Weinberg–Salam theory. A natural understanding of quark confinement based on lattice gauge theory has convinced people that QCD certainly describes the strong interaction. Now, as the Standard Model is being confirmed with higher and higher accuracy by the precise experiments at LEP, we may say that our understanding of field theory at the perturbative level is quite sufficient. On the other hand, we should say that there remains much to be clarified concerning the non–perturbative effects. Studying the dynamics of quantum gravity is important also from this point of view, and we hope that its progress will greatly help us understand the non–perturbative features of field theory.

There has been considerable progress in two dimensional quantum gravity [1] based on a continuum formulation — Liouville theory [2] — and a kind of lattice formulation — dynamical triangulation [3]. Both have been exactly solved and their equivalence has been established [4]. However, the theories which have been solved so far are still kinds of toy model. In the context of string theory, we have to break the so–called $c = 1$ barrier in order to study the critical string. In the context of ordinary field–theoretical approach to quantum gravity, we have to study the system in higher dimensions. Although it goes without saying that it is desirable to develop an analytic approach to these difficult problems, numerical approach seems to be

indispensable. We can quote the numerical work done by Creutz [5] in the early 80's. It was shown numerically that the confinement, which was proved by Wilson [6] in the strong–coupling limit, survives in the continuum limit for non–Abelian gauge theories in four dimensions. Unfortunately, in the case of quantum gravity, we do not know a good observable such as Wilson loop in gauge theory. We may expect, however, that we can obtain qualitative information on the system through numerical simulations, which we hope will eventually enable us to study interesting features of quantum gravity in the continuum limit.

1.2 Dynamical triangulation v.s. Regge calculus

Let us explain what kind of system we work on throughout this thesis. We consider a D–dimensional manifold with fixed topology, on which we introduce the metric $g_{\mu\nu}$ with Euclidean signature and the matter field φ. The partition function is written as

$$Z = \int \frac{\mathcal{D}g\mathcal{D}\varphi}{\mathrm{vol(Diff)}} \, \mathrm{e}^{-(S_{\mathrm{G}}[g]+S_{\mathrm{M}}[g,\varphi])}, \tag{1.1}$$

where the actions are given by

$$S_{\mathrm{G}} = \int \mathrm{d}^D x\sqrt{g}(\Lambda - \frac{1}{G}R) \tag{1.2}$$

$$S_{\mathrm{M}} = \int \mathrm{d}^D x\sqrt{g}(g^{\mu\nu}\partial_\mu\varphi\partial_\nu\varphi + m^2\varphi^2), \tag{1.3}$$

and the measure is defined through the norm

$$||\delta g||^2 = \int \mathrm{d}^D x\sqrt{g}g^{\mu\nu}g^{\lambda\rho}\delta g_{\mu\lambda}\delta g_{\nu\rho} \tag{1.4}$$

$$||\delta\varphi||^2 = \int \mathrm{d}^D x\sqrt{g}(\delta\varphi)^2. \tag{1.5}$$

Since this theory possesses the diffeomorphism invariance, we have to divide the measure by vol(Diff) which represents the gauge volume corresponding to the diffeomorphism invariance.

Let us consider the two–dimensional case. Note that in two dimensions, the Einstein term gives the Euler number χ,

$$\int \mathrm{d}^2 x\sqrt{g}R = 2\pi\chi, \tag{1.6}$$

so that the action for the gravity sector includes only the cosmological term. Let us take the conformal gauge [2],

$$g_{\mu\nu} = \hat{g}_{\mu\nu}(\tau)\mathrm{e}^{\phi(x)}, \tag{1.7}$$

where $\hat{g}_{\mu\nu}$ is some given background metric parametrized with the moduli parameter τ. One can then consider the dynamics of ϕ on the curved space specified with the background metric $\hat{g}_{\mu\nu}$. This is the Liouville theory which has been studied analytically with great success in the late 80's [2]. The strategy is to require that the theory of ϕ on the curved space should be independent of the background metric $\hat{g}_{\mu\nu}$, which ensures the general covariance of the original theory.

Let us next consider a kind of lattice regularization in quantum gravity. It is important for us to see if we can reproduce the results of the continuum theory by first regularizing the theory in a rigorous way and then taking the continuum limit. Such a constructive formalism is indispensable not only in understanding the universality of the theories, but also in investigating the dynamics of the theories through numerical simulation. In the case of ordinary field theory, we use a regular lattice and put the matter field on each site. The gauge field can be put on each link so that the gauge invariance is manifestly realized on the lattice. By doing this, the fluctuations of the fields are cutoff by the lattice spacing. Although the rotational and translational invariances are broken to the discrete ones, it is numerically confirmed that they are restored in the continuum limit.

Let us consider this kind of regularization in quantum gravity. Since here the space–time itself is the dynamical object, we have to introduce a scale within which the fluctuations of the manifold are forbidden. Except for this restriction, the path integral should be performed over all the manifolds. A formulation that realizes this idea most naturally is the dynamical triangulation, in which the path integral over the metric is replaced with summation over all the piecewise–flat manifolds made up with equilateral D–simplices. It is certainly not trivial if this philosophy really gives the general covariance in the continuum limit. In two dimensions, however, dynamical triangulation has been treated analytically [3] and it has been shown

that one can take a sensible continuum limit, which gives the same results as the continuum approach [4]. This encourages us to use dynamical triangulation as a regularization of quantum gravity also in higher dimensions. We may naturally expect that if one can obtain a sensible continuum limit, the theory possesses the general covariance. Although analytical treatment in the case of higher dimensions may be difficult, there is no potential obstacle in numerical approach through Monte Carlo simulations. However, in contrast to ordinary statistical systems, we have to change the lattice structure dynamically, which makes it difficult for us to write an efficient code with vectorization etc..

There is another type of lattice regularization of quantum gravity which is called Regge calculus [9, 10]. In this formalism, the triangulation is fixed and the path integral over the metric is replaced with path integral over the link lengths with the constraint of triangle inequality. It has a practical advantage to dynamical triangulation, since we can vectorize the code as in ordinary statistical systems. However, there are many problems in this formalism. First of all, it is not clear what kind of measure should be chosen for the link–length integral. Secondly we do not know how to introduce the cutoff in a natural way as in dynamical triangulation. Finally, this formalism does not have any grounds for the appearance of general covariance in the continuum limit. There is an argument that in Regge calculus the general covariance is trivial as well as in dynamical triangulation, since the description does not depend on any specific coordinate, and it is a completely geometrical object that is being dealt with. This is not correct, however. The general covariance in this sense is nothing but the classical one, which even ordinary field theories on a curved space also possess. Therefore, it does not specify how the metric should fluctuate in any sense.

This thesis is organized as follows. In Chapter 2, we address the problem of general covariance in Regge calculus. Since we have analytic results from Liouville theory and/or dynamical triangulation in two dimensions, whether we can reproduce them also from Regge calculus serves as a test of the formalism. There has been two works done in this direction recently [12, 13], both of them reporting negative

results. We claim that the quantities they measured are not unambiguously defined in Regge calculus. We point out that the fractal structure studied in Ref. [15] in the continuum limit of dynamical triangulation is completely well–defined also in Regge calculus and that we can measure it through numerical simulation [14]. We perform a large size simulation of quantum Regge calculus and show that it reproduces the expected loop–length distribution for the type of loops that is attached to baby universes, when the scale–invariant measure is adopted. This suggests the possibility that Regge calculus might restore the general covariance in the continuum limit if the measure of the link–length integration is properly chosen. In Chapter 3, we consider the problem of constructing quantum gravity in dimensions greater than two. We first review briefly the recent progress [28, 29] in the ϵ–expansion approach to this problem, which suggests that quantum gravity can be constructed at least by ϵ–expansion around two dimensions. We then review the basic observations in the numerical simulation based on dynamical triangulation [33, 34, 35, 36, 37]. Although it is promising that we observe a second order phase transition in four dimensions, it is still unclear whether we can take a sensible continuum limit at the critical point. We then present our recent results in four dimensions [39]. We measure vertex–order distribution and show that, in the strong–coupling phase, there is a vertex with very large order. We then put in the action an additional term which suppresses the vertex with very large order, and observe that the system is always in the branched– polymer phase. We also present a clue that the branched–polymer structure is related to the conformal–mode instability. Chapter 4 is devoted to the summary and discussion.

Chapter 2

Two–dimensional quantum Regge calculus

2.1 Introduction

The success in two-dimensional quantum gravity is based on a continuum formulation — Liouville theory [2] — and a kind of lattice formulation — dynamical triangulation [3]. Both have been exactly solved and their equivalence has been established [4]. In the case of ordinary quantum field theories, continuum formulations and lattice formulations have played complementary roles in understanding the universality in field theory. The details of lattice formulations at the lattice level are irrelevant to the long-range behavior of the theory, which can be also described in terms of a continuum formulation. A natural explanation of the universality has been given by the concepts of the renormalization group [7]. The equivalence of Liouville theory and dynamical triangulation in two-dimensional quantum gravity suggests that the universality exists also in quantum gravity. In fact, some kinds of universality are known in dynamical triangulation; the continuum limit is not affected by using squares instead of triangles as the building blocks or by prohibiting tadpoles or self-energies in the dual diagram, etc.. Although we still lack understanding of the universality in quantum gravity in terms of the renormalization group, invention of such a framework (for some attempts, see [8]) might be especially useful in studying quantum gravity in three or four dimensions, where there is no analytic solution.

To this end, it seems quite important for us to investigate the universality phenomena further in two-dimensional quantum gravity. For example, Regge calculus provides another type of lattice regularization of quantum gravity, although the appearance of the general covariance is quite nontrivial in such a formalism with fixed lattice structure. An interesting question to ask here is whether two-dimensional Regge calculus falls into the same universality class as dynamical triangulation and Liouville theory. The answer is also desired from a practical point of view, since Regge calculus might be useful for numerical simulations of quantum gravity in higher dimensions.

Since analytic treatment of Regge calculus seems difficult beyond a perturbative expansion around flat space-time [10], we investigate the above issue by numerical simulation. There have been several works in this direction. A few years ago, Gross and Hamber [11] reported that Regge calculus reproduced the string susceptibility known in dynamical triangulation and in the continuum theory. Recently, Bock and Vink [12] have performed a more careful analysis and have claimed that Regge calculus fails to reproduce the desired string susceptibility. It has been also reported [11, 13] that the critical exponents of the Ising model on the dynamical Regge lattice agree quite well with the ones of the Ising model on the static lattice (Onsager's values) and not with the ones of the Ising model on the dynamically triangulated lattice. We think, however, that all these works are subject to some subtleties in Regge calculus concerning either the definition of string susceptibility or the introduction of matter fields, as we explain later.

In order to compare Regge calculus with the other approaches unambiguously, it is desirable to have a universal quantity which can be calculated directly from

the geometry of the surface. Indeed, such a quantity exists; it is the so-called loop-length distribution, which has been studied by Kawai, Kawamoto, Mogami and Watabiki [15]. They constructed a transfer-matrix formalism in dynamical triangulation. Using the formalism, they succeeded in obtaining the loop-length distribution in the continuum limit, which characterizes the fractal structure of the surface. The loop-length distribution can be defined unambiguously also in Regge calculus and it can be measured through numerical simulation. We, therefore, examine the loop-length distribution in a numerical simulation of Regge calculus and compare the result with that obtained in the continuum limit of dynamical triangulation.

2.2 Definition of the system

Let us first explain the system we consider in this chapter. In Regge calculus the dynamical variables are the link lengths on a fixed triangulation. Since it is essential for our purpose to have a spherical topology, we construct the fixed triangulation by dividing each of the twenty surfaces of an icosahedron into a triangular lattice. A tetrahedron or octahedron could be used as well, but we have chosen an icosahedron so that the artifact of the non-uniformity of coordination number may be the minimum. The integration over the link lengths is performed taking either the uniform measure $\int \prod_i \mathrm{d}l_i$ or the scale-invariant measure $\int \prod_i \mathrm{d}l_i/l_i$. The triangle inequality is imposed on every triangle.

The total area is fixed to be equal to the number of triangles, so that the average area of a triangle in each configuration becomes unity. This can be realized in the simulation as follows. We first consider a system with the measure $\int \prod_i \mathrm{d}l_i\, {l_i}^{p-1}$ and the action $S = \lambda A$, where A is the total area of the surface and λ is a constant parameter. $p = 1$ corresponds to the uniform measure and $p = 0$ corresponds to the scale-invariant measure. The partition function is given by

$$Z(\lambda) = \int \prod_i \mathrm{d}l_i\, {l_i}^{p-1}\, \mathrm{e}^{-\lambda A}\, \Theta(\textit{triangle inequalities}), \tag{2.1}$$

where $\Theta(\textit{triangle inequalities})$ is the step function which gives one if all the triangle inequalities are satisfied and zero otherwise. Changing the variables of integration as $l_i \to l_i/\sqrt{\lambda}$, one can extract the explicit λ-dependence of $Z(\lambda)$ as

$$Z(\lambda) = \frac{1}{\left(\sqrt{\lambda}\right)^{pN_{\mathrm{link}}}} \int \prod_i \mathrm{d}l_i\, {l_i}^{p-1}\, \mathrm{e}^{-A}\, \Theta(\textit{triangle inequalities}), \tag{2.2}$$

where N_{link} is the number of links. Inverse Laplace transform of eq. (2.1) gives the distribution of the total area as

$$\varphi(A) \propto \mathrm{e}^{-\lambda A} A^{\frac{pN_{\mathrm{link}}}{2}-1}. \tag{2.3}$$

For the uniform measure ($p = 1$), we control the total area by introducing a positive λ, while for the scale-invariant measure ($p = 0$), we set $\lambda = 0$ and rescale the configuration whenever necessary during the simulation so that the total area may be kept within a range of moderate value. The configurations thus generated for either measure are each rescaled before measurements to have the fixed total area equal to the number of triangles.

We have performed Monte Carlo simulations using the heat-bath algorithm with 50,000 triangles for the uniform measure and with 12,500, 50,000 and 200,000 triangles for the scale-invariant measure. The updating process in the program is vectorized since we can update one third of the links independently at the same time.

2.3 Subtleties in Regge calculus

Before proceeding, we would like to explain the subtleties in Regge calculus. The first point is the definition of string susceptibility. In dynamical triangulation, the string susceptibility γ_{str} can be defined through

$$Z(N) = \sum_{T \in \mathcal{T}_N} \mathrm{e}^{-S(T)} \sim N^{\gamma_{\mathrm{str}}-3} \mathrm{e}^{\kappa N} \qquad (N \to \infty), \tag{2.4}$$

where $\mathcal{T}_N$ denotes the set of triangulations with N triangles [16]. In Regge calculus, the partition function for a fixed triangulation with N triangles can be written as

$$Z(A,N) = \int \mathrm{d}\mu(\{l_i\})\ \mathrm{e}^{-S(\{l_i\})}\ \delta(A(\{l_i\}) - A)\ \Theta(\textit{triangle inequalities}), \qquad (2.5)$$

where $\mathrm{d}\mu(\{l_i\})$ denotes the measure for the link-length integration, and $A(\{l_i\})$ denotes the total area of the surface, which is fixed to a given value A. In refs. [11, 12], they defined the string susceptibility in Regge calculus through

$$Z(A,N) \sim A^{\gamma_{\mathrm{str}}-3}\mathrm{e}^{\kappa A} \qquad (A \to \infty), \qquad (2.6)$$

for a fixed N, which is taken to be sufficiently large. This definition of string susceptibility, however, might be too naive. When we consider a scaling relation in field theory, we have to keep the cutoff of the theory constant. In Regge calculus, we have no definite quantity that corresponds to the cutoff in ordinary field theory, and therefore the scaling argument is rather subtle. One natural thing to do is to consider the average area of a triangle in each configuration as the cutoff in ordinary field theory. In order to keep the cutoff constant, say at unity, we should fix the total area A to be equal to the number of triangles N. The string susceptibility, then, can be defined through

$$Z(A=N,N) \sim N^{\gamma_{\mathrm{str}}-3}\mathrm{e}^{\kappa N} \qquad (N \to \infty). \qquad (2.7)$$

Unfortunately, the string susceptibility thus defined seems to be difficult to extract from numerical simulation, since we have to probe the difference in free energy for different numbers of triangles.

The second point is the introduction of matter fields. If we assign a single spin to each triangle, each spin should be regarded as a representative ("block spin") of the dynamical degrees of freedom within the triangle. Therefore, we may have to, for example, make the Ising coupling constant dependent on the size of the triangle, which takes a different value from point to point in Regge calculus. Thus the negative results obtained in ref. [11, 13] might be due to the problem of the action for the matter fields.

In contrast to the above points, the loop-length distribution can be defined unambiguously in Regge calculus and we hope this provides us with a definite criterion whether Regge calculus serves as a proper regularization of quantum gravity.

2.4 Loop–length distribution

Let us explain the loop-length distribution, which plays a central role in our study. The set of points which are at a distance D from a given point is composed of a number of disconnected closed loops. The distribution $\rho(L,D)$ of the loop length L at the distance D has been obtained in the continuum limit of dynamical triangulation as [15]

$$\rho(L,D) = \frac{1}{D^2} f(x) \qquad (2.8)$$

$$f(x) = \frac{3}{7\sqrt{\pi}}\left(x^{-\frac{5}{2}} + \frac{1}{2}x^{-\frac{3}{2}} + \frac{14}{3}x^{\frac{1}{2}}\right)\mathrm{e}^{-x}, \qquad (2.9)$$

where $x = L/D^2$. The fact that such a quantity does possess a sensible continuum limit is not only quite non-trivial itself but also of great significance since it provides us with a geometrical picture of the continuum limit of quantum gravity. It implies that in the continuum limit of quantum gravity, the space-time becomes fractal in the sense that sections of the surface at different distances from a given point look exactly the same after a proper rescaling of loop lengths. Let us here consider the distribution of loops with length L attached to a universe with area A'. This can be written in terms of the functions given in ref. [15] as,

$$\rho(L,A';D;A) = \lim_{L_0\to 0} \frac{\frac{1}{2\pi i}\int \mathrm{d}\tau' N(L_0,L;D;\tau')\mathrm{e}^{\tau'(A-A')}\frac{1}{2\pi i}\int \mathrm{d}\tau''\frac{1}{L}F(L,\tau'')\mathrm{e}^{\tau''A'}}{\frac{1}{2\pi i}\int \mathrm{d}\tau''\frac{1}{L_0}F(L_0,\tau'')\mathrm{e}^{\tau''A}}, \qquad (2.10)$$

where A is the total area of the surface. When we take the thermodynamic limit $A \to \infty$, we can fix either A' or $(A - A')$ to a finite value B. The former corresponds to the type of loop attached to a baby universe, while the latter corresponds to the type of loop attached to the mother universe. We refer to the two types of loops simply as "baby" loops and "mother" loops, respectively (fig. 1).

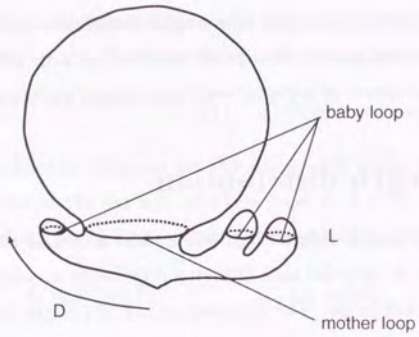

Figure 1: The loops appearing at the distance D from a given point. There are two types of loops : the "mother" loop which is attached to the mother universe, and "baby" loops which are attached to baby universes.

Note that baby loops are not necessarily smaller than mother loops. The distribution for baby loops can be calculated as follows,

$$\rho_{\rm b}(L,B;D) = \frac{1}{2\pi i}\int {\rm d}\tau' {\rm e}^{\tau' B} \lim_{L_0\to 0,\tau\to 0} \frac{\frac{\partial^2}{\partial\tau^2}N(L_0,L;D;\tau)\frac{1}{L}F(L,\tau+\tau')}{\frac{\partial^2}{\partial\tau^2}\frac{1}{L_0}F(L_0,\tau)} \quad (2.11)$$

$$= \frac{1}{D^6}\frac{6}{7\pi}\left(1+\frac{1}{2}x\right){\rm e}^{-x}x^{\frac{1}{2}}y^{-5}{\rm e}^{-\left(\frac{x}{y}\right)^2}, \quad (2.12)$$

where $x = L/D^2$ and $y = \sqrt{B}/D^2$. Integrating over B, one gets,

$$\rho_{\rm b}(L,D) = \int_0^\infty \rho_{\rm b}(L,B;D){\rm d}B \quad (2.13)$$

$$= \frac{1}{D^2}f_{\rm b}(x), \quad (2.14)$$

where

$$f_{\rm b}(x) = \frac{3}{7\sqrt{\pi}}\left(x^{-\frac{5}{2}}+\frac{1}{2}x^{-\frac{3}{2}}\right){\rm e}^{-x}. \quad (2.15)$$

The distribution for mother loops can be calculated similarly.

$$\rho_{\rm m}(L,B;D)$$

$$= \frac{1}{2\pi i}\int {\rm d}\tau' {\rm e}^{\tau' B} \lim_{L_0\to 0,\tau\to 0} \frac{\frac{\partial^2}{\partial\tau^2}N(L_0,L;D;\tau+\tau')\frac{1}{L}F(L,\tau)}{\frac{\partial^2}{\partial\tau^2}\frac{1}{L_0}F(L_0,\tau)}$$

$$= \frac{1}{\sqrt{\pi L}}\frac{\partial}{\partial D}\left[\frac{1}{2\pi i}\int_{-i\infty}^{i\infty}{\rm d}\tau {\rm e}^{\tau B}\exp\left\{-\frac{\sqrt{\tau}L}{2}\left(3\tanh^{-2}\frac{\sqrt{6\sqrt{\tau}}D}{2}-2\right)\right\}\right] \quad (2.16)$$

Integrating over B, one gets,

$$\rho_{\rm m}(L,D) = \int_0^\infty \rho_{\rm m}(L,B;D){\rm d}B \quad (2.17)$$

$$= \frac{1}{\sqrt{\pi L}}\frac{\partial}{\partial D}\lim_{\tau\to 0}\exp\left\{-\frac{\sqrt{\tau}L}{2}\left(3\tanh^{-2}\frac{\sqrt{6\sqrt{\tau}}D}{2}-2\right)\right\} \quad (2.18)$$

$$= \frac{1}{D^2}f_{\rm m}(x), \quad (2.19)$$

where

$$f_{\rm m}(x) = \frac{2}{\sqrt{\pi}}x^{\frac{1}{2}}{\rm e}^{-x}. \quad (2.20)$$

The total distribution reproduces the result of ref. [15] [1], *i.e.* $\rho(L,D) = \rho_{\rm b}(L,D) + \rho_{\rm m}(L,D)$. Note that the integration of the mother-loop distribution over L gives

$$\int_0^\infty \rho_{\rm m}(L,D){\rm d}L = \frac{2}{\sqrt{\pi}}\int_0^\infty x^{\frac{1}{2}}{\rm e}^{-x}{\rm d}x = 1, \quad (2.21)$$

which means that one finds exactly one mother loop at a fixed D in each configuration.

In Regge calculus we define the loop-length distribution in the following way. Representing each triangle by the center of its inscribed circle, we define the length of a dual-link by the geodesic distance of the two representative points at the ends of the dual-link. Then we define the distance between two given triangles by the length of the shortest dual-link path connecting the two triangles (fig. 2).

[1] The fact that the loop-length distribution is composed of two such contributions can also be seen from eq.(24) of ref. [15]. One can get the singularity $\tau^{3/2}$ in the numerator either from the proper-time evolution kernel $N(L_0,L;D)$ or from the disk amplitude $F(L)$. The former contribution corresponds to baby loops, while the latter to mother loops [17].

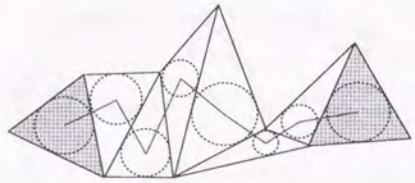

Figure 2: An example of a dual-link path connecting the two shaded triangles. The distance between the two triangles is defined by the length of the shortest dual-link path.

The boundary between triangles at a distance less than or equal to D from a given triangle and those at a distance greater than D from the same triangle is composed of disconnected closed loops, whose lengths are defined by summing up the lengths of the links forming each loop. This gives the definition of the loop-length distribution in Regge calculus. Since we are dealing with a finite number of triangles, we have a maximum D at which all the triangles are included. We measure the loop-length distribution at D's which are less than half of the maximum D. Also the finiteness of the system makes the classification of loops into baby loops and mother loops somewhat ambiguous. We identify the mother loop with the loop attached to the largest universe at a fixed D. The measurement has been made every 200 sweeps, and at each measurement we choose ten triangles randomly as the starting point of the distance D in order to increase the statistics. The number of sweeps required for the thermalization of the data is large for the scale-invariant measure; *e.g.* 500,000 sweeps in the case of 12,500 triangles.

2.5 Results of the simulation

Let us show the results of our simulation. The data for the uniform measure $(\int \prod_i dl_i)$ with 50,000 triangles is shown in Fig. 3.

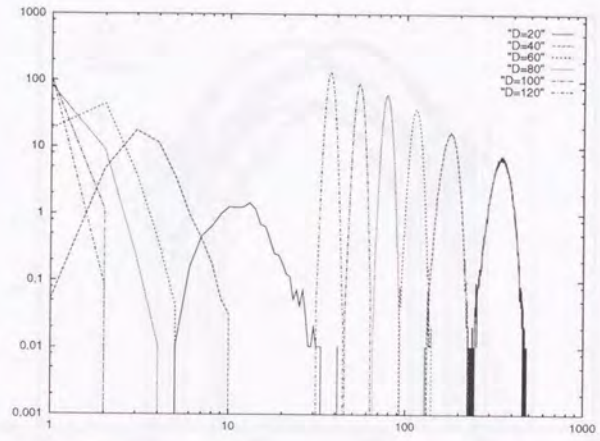

Figure 3: The loop-length distribution for the uniform measure $(\int \prod_i \mathrm{d}l_i)$ with 50,000 triangles. The horizontal axis is the scaling variable $x = L/D^2$.

The loop-length distribution is plotted against the scaling variable $x = L/D^2$ for $D = 20, 40, 60, 80, 100, 120$, where L is the length of the loop and D is the distance from a point on the surface. The result does not show any scaling behavior in terms of x for different values of D. The distribution for each D is split into two parts: the left one which corresponds to baby loops and the right one which corresponds to mother loops. One should note that it is a log-log plot, and so we see that the baby loops are extremely suppressed. Indeed, for most cases we find only one loop, which is the mother loop, for each D in a configuration. (A baby loop appears on average only once in five configurations even for $D = 120$.) This means that the surface is rather similar to a smooth sphere, where always only one loop (which is the mother loop) appears. Hence the surface is quite different from being fractal as in dynamical triangulation, where many loops appear for each D.

The data for the scale-invariant measure $(\int \prod_i dl_i/l_i)$ with 12,500 triangles is shown in Fig. 4.

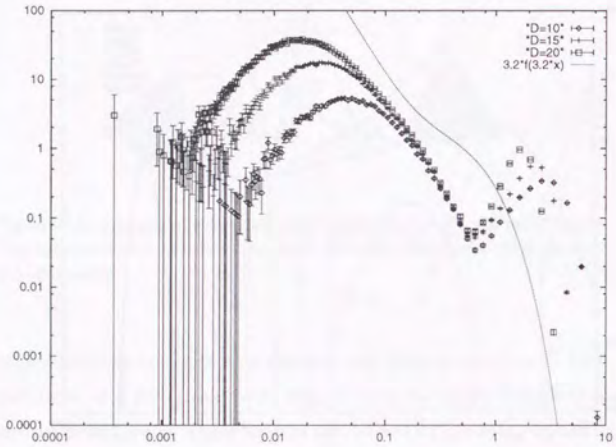

Figure 4: The loop-length distribution for the scale-invariant measure $(\int \prod_i \mathrm{d}l_i/l_i)$ with 12,500 triangles. The horizontal axis is the scaling variable $x = L/D^2$. The dotted curve is the rescaled universal function $\alpha f(\alpha x)$ with the same $\alpha = 3.2$ that gives the best fit in the case of the baby-loop distribution (Fig. 5).

The loop-length distribution is plotted against the scaling variable $x = L/D^2$ for $D = 10, 15, 20$. Something of a scaling behavior is seen in the intermediate region of x. To clarify the situation, we separate the two contributions, the one from baby loops and the one from mother loops. The distribution for baby loops is shown in Fig. 5.

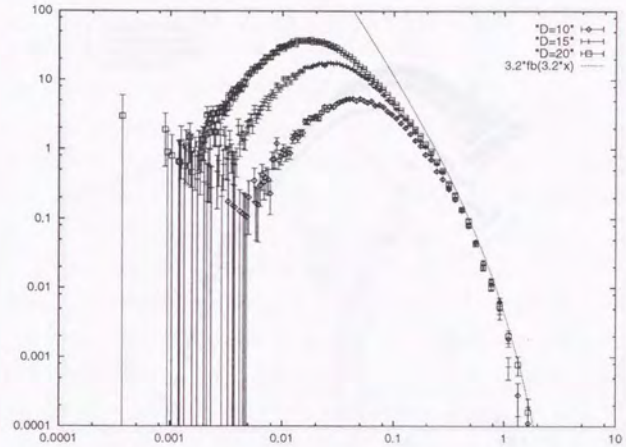

Figure 5: The baby-loop length distribution for the scale-invariant measure$(\int \prod_i \mathrm{d}l_i/l_i)$ at $D = 10, 15, 20$ with 12,500 triangles. The horizontal axis is the scaling variable $x = L/D^2$. The dotted curve is the rescaled universal function $\alpha f_{\mathrm{b}}(\alpha x)$ with $\alpha = 3.2$ which gives the best fit.

A clear scaling behavior can be seen with $x = L/D^2$ as a scaling parameter. Furthermore, we compare our result with the universal function (2.15) obtained in the continuum limit of dynamical triangulation. Since there is an ambiguity by a constant factor between the scaling parameter x in our system and that in eq. (2.15), we fit our result with $\alpha f_{\mathrm{b}}(\alpha x)$, where α is the fitting parameter. The best fit ($\alpha = 3.2$) is shown by the dotted line in Fig. 5. Our data is in good agreement with the universal function. Let us see how the slight discrepancy seen in the small-x region behaves as we increase the number of triangles N. Fig. 6 shows the results for $D = 20$ with 12,500, 50,000 and 200,000 triangles.

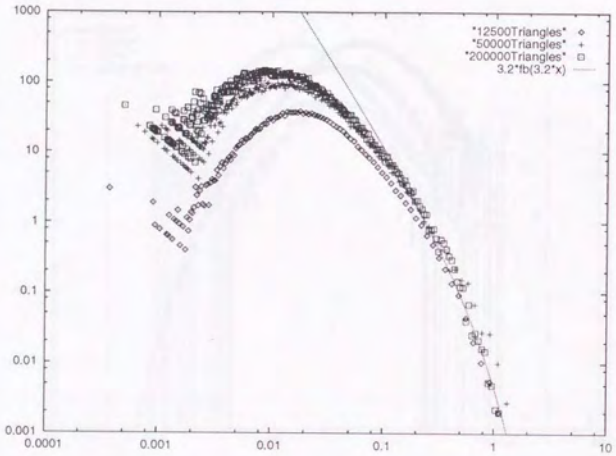

Figure 6: The baby-loop length distribution for the scale-invariant measure($\int \prod_i \mathrm{d}l_i/l_i$) at $D = 20$ with 12,500, 50,000, 200,000 triangles. The horizontal axis is the scaling variable $x = L/D^2$.

We find that the data curve in the small-x region approaches to the curve of the universal function (2.15). Thus we expect that the distribution of baby loops will converge to the universal function in the $N \to \infty$ limit. The distribution for mother loops, on the other hand, is shown in Fig. 7 and Fig. 8, which correspond to the cases with 12,500 triangles and 200,000 triangles respectively.

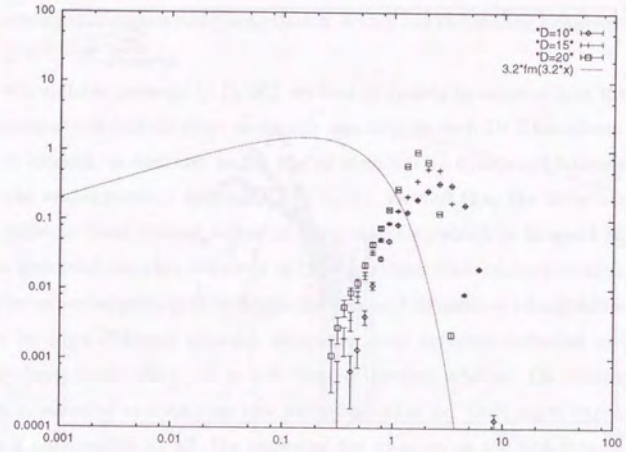

Figure 7: The mother-loop length distribution for the scale-invariant measure ($\int \prod_i \mathrm{d}l_i/l_i$) at $D = 10, 15, 20$ with 12,500 triangles. The horizontal axis is the scaling variable $x = L/D^2$. The dotted curve is the rescaled universal function $\alpha f_{\mathrm{m}}(\alpha x)$ with the same $\alpha = 3.2$ that gives the best fit in the case of the baby-loop distribution.

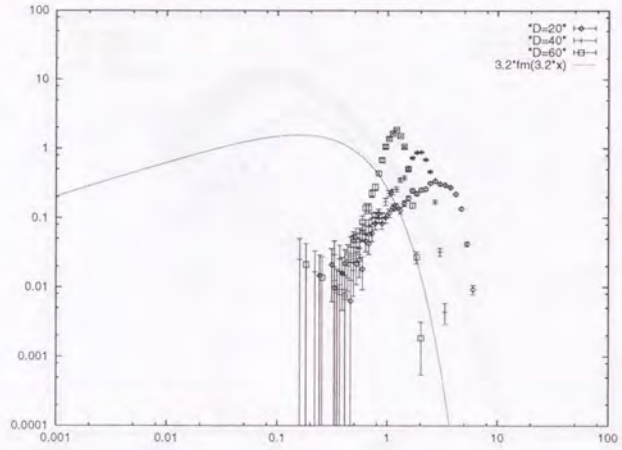

Figure 8: The mother-loop length distribution for the scale-invariant measure $(\int \prod_i \mathrm{d}l_i/l_i)$ at $D = 20, 40, 60$ with 200,000 triangles. The horizontal axis is the scaling variable $x = L/D^2$.

We cannot see any scaling behavior here. The dotted line represents the rescaled universal function $\alpha f_{\mathrm{m}}(\alpha x)$ with the same $\alpha = 3.2$ that gives the best fit in the case of the baby-loop distribution. Although we might expect that the data will approach the universal function for larger D with sufficiently many triangles, the finite-size effect in the present data is too severe for us to draw any conclusion.

2.6 Summary of this chapter

To summarize, we have performed a Monte Carlo simulation of two-dimensional Regge calculus up to 200,000 triangles and measured the loop-length distribution, which is the distribution function of the length L of the loops whose geodesic distance from a point is a constant D. The results are compared with that obtained in the

continuum limit of dynamical triangulation, which has the scaling behavior in terms of $x = L/D^2$.

For the uniform measure $(\int \prod_i dl_i)$, we find no scaling in terms of x at the present size. Moreover, we find for most cases only one loop for each D. This means that the surface is smooth, in contrast to the fractal structure in dynamical triangulation.

For the scale-invariant measure $(\int \prod_i \mathrm{d}l_i/l_i)$, we find that the baby-loop distribution shows a clear scaling behavior in terms of x, which is in good agreement with the universal function obtained in the continuum limit of dynamical triangulation. It is rather surprising that Regge calculus and dynamical triangulation, which seem to be quite different systems, show the same universal behavior at least for the baby-loop distribution. It is not clear at present whether the scale-invariant measure is essential in obtaining this universal behavior. One might expect that if there is a universality at all, the choice of the measure of the link-length integration would be irrelevant to the universal behavior. We should note, however, that the scale-invariant measure is very special, as is seen in eq. (2.3). It implies that the fluctuation of the area of each triangle becomes overwhelmingly large when the scale-invariant measure is adopted. Since the lattice structure is regular in Regge calculus, such a large fluctuation might be necessary to obtain a fractal structure as in dynamical triangulation.

As for the mother-loop distribution, the situation is not clear even for the scale-invariant measure. We feel it is possible that the mother-loop distribution, as well as the baby-loop distribution, converges to the universal function in the $N \to \infty$ limit. Even if this turns out to be the case, we may at least say that Regge calculus requires many more triangles in order to obtain the universal behavior than dynamical triangulation, which is known to show a fairly good universal fractal structure with no more than 20,000 triangles [18].

Chapter 3

Higher–dimensional quantum gravity

3.1 Problems in higher–dimensional quantum gravity

In this chapter, we consider the possibility of constructing a consistent theory of quantum gravity in dimensions greater than two. Let us first discuss the problems in such an attempt within perturbation theory. In this and the next section, we use the 't Hooft–Veltman convention [19] i.e.

$$R^{\mu}{}_{\nu\lambda\rho} = \partial_\lambda \Gamma^{\mu}{}_{\nu\rho} - \cdots, \tag{3.1}$$

$$R_{\nu\lambda} = R^{\mu}{}_{\nu\lambda\mu}, \tag{3.2}$$

$$R = g^{\nu\lambda} R_{\nu\lambda}, \tag{3.3}$$

which is commonly used in perturbative calculations. Note that the sign of the curvature is opposite to the one used in the other sections. Let us consider Einstein

gravity, which is described by the action

$$S = \frac{1}{G}\int \mathrm{d}^D x \sqrt{g} R. \tag{3.4}$$

We parametrize the metric as

$$g_{\mu\nu} = \tilde{g}_{\mu\nu} \mathrm{e}^{-\phi} = \hat{g}_{\mu\rho} (\mathrm{e}^h)^{\rho}{}_{\nu} \mathrm{e}^{-\phi}, \tag{3.5}$$

where $\hat{g}_{\mu\nu}$ is the background metric and $h^{\mu}{}_{\nu}$ is the traceless symmetric tensor field. We call ϕ the conformal mode and $h^{\mu}{}_{\nu}$ the transversal mode. Then the Einstein action can be written in terms of ϕ and h as

$$\begin{aligned} S &= \frac{1}{G}\int \mathrm{d}^D x \sqrt{\hat{g}} \mathrm{e}^{-(\frac{D}{2}-1)\phi} [\tilde{R} - (D-1)\tilde{g}^{\mu\nu}\tilde{\nabla}_{\mu}\partial_{\nu}\phi \\ &\qquad + \frac{1}{4}(D-2)(D-1)\tilde{g}^{\mu\nu}\partial_{\mu}\phi\partial_{\nu}\phi]. \qquad (3.6) \\ &= \frac{1}{G}\int \mathrm{d}^D x \sqrt{\hat{g}} \mathrm{e}^{-(\frac{D}{2}-1)\phi} [\tilde{R} - \frac{1}{4}(D-2)(D-1)\tilde{g}^{\mu\nu}\partial_{\mu}\phi\partial_{\nu}\phi] \\ &\qquad + \text{total derivative}. \qquad (3.7) \end{aligned}$$

$\tilde{R}$ is the scalar curvature made out of $\tilde{g}_{\mu\nu}$ and it can be written in terms of h as

$$\tilde{R} = \hat{R} - h^{\mu\nu}\hat{R}_{\mu\nu} - h^{\mu\nu}{}_{;\mu\nu} + \frac{1}{4} h^{\mu\nu}{}_{;\lambda} h_{\mu\nu;}{}^{\lambda} + \cdots, \tag{3.8}$$

The overall signature of the action has been chosen so that the transversal mode is bounded from below. Then we find that the kinetic term for the conformal mode has the wrong sign. If ϕ fluctuates around 0 very violently, the action can take arbitrarily large negative value. This means that the action is unbounded, which might cause a problem in Euclidean path integral formalism [20].

As is well known, the theory is unrenormalizable for $D > 2$, since the dimension of the coupling constant G is $2 - D$. It means that the coupling becomes uncontrollably large at short distance and the renormalization program in perturbation theory breaks down.

The situation resembles that of non–linear sigma model, whose action is written as

$$S = \frac{1}{f}\int \mathrm{d}^D x \partial_{\mu}\vec{\sigma}\partial_{\mu}\vec{\sigma}, \tag{3.9}$$

where $\vec{\sigma}$ is a N–dimensional unit vector. The above action possesses $O(N)$ symmetry. Let us assume that this symmetry is spontaneously broken in the weak coupling region and consider a perturbation around $\vec{\sigma} = (1, 0, \cdots, 0)$. We parametrize the σ field as $\vec{\sigma} = (\sqrt{1-\vec{\pi}^2}, \vec{\pi})$, where $\vec{\pi}$ is a $(N-1)$–dimensional vector. The action, then, becomes

$$S = \frac{1}{f}\int \mathrm{d}^D x \partial_\mu \vec{\pi}\partial_\mu \vec{\pi} + \frac{1}{1-\vec{\pi}^2}(\vec{\pi}\partial_\mu\vec{\pi})(\vec{\pi}\partial_\mu\vec{\pi}). \tag{3.10}$$

In order to make the kinetic term canonical, let us rescale the π field as $\vec{\pi} \to \sqrt{f}\vec{\pi}$.

$$S = \int \mathrm{d}^D x \partial_\mu \vec{\pi}\partial_\mu \vec{\pi} + f\frac{1}{1-f\vec{\pi}^2}(\vec{\pi}\partial_\mu\vec{\pi})(\vec{\pi}\partial_\mu\vec{\pi}). \tag{3.11}$$

Since the dimension of f is $2-D$, this theory is unrenormalizable for $D > 2$.

However, as is well known, three-dimensional non-linear sigma model can be defined constructively as follows. We put the theory on a lattice with the action

$$\begin{aligned} S_{\mathrm{lat}} &= \frac{1}{af_{\mathrm{lat}}}a^3 \sum_n \sum_{\hat{\mu}=1}^{3} (\frac{\vec{\sigma}_n - \vec{\sigma}_{n+\hat{\mu}}}{a})^2 \\ &= -\frac{2}{f_{\mathrm{lat}}}\sum_{n,\hat{\mu}} \vec{\sigma}_n\vec{\sigma}_{n+\hat{\mu}} + \mathrm{const.} \end{aligned} \tag{3.12}$$

This is nothing but the ferromagnetic system and it undergoes a second order phase transition at a critical point $f_{\mathrm{lat}} = f_{\mathrm{lat}}^{\mathrm{crit}}$. Below the critical point, the $O(N)$ symmetry is spontaneously broken and $\langle\vec{\sigma}\rangle \neq 0$, whereas above the critical point, the system is in the symmetric phase and $\langle\vec{\sigma}\rangle = 0$. We can take a continuum limit at the critical point. Actually this theory belongs to the same universality class as three-dimensional $O(N)$ symmetric ϕ^4 theory, which is perturbatively renormalizable. This fact can be understood as follows. The action of $O(N)$ symmetric ϕ^4 theory can be given as

$$S = \int \mathrm{d}^D x \partial_\mu\vec{\phi}\partial_\mu\vec{\phi} + m^2\vec{\phi}^2 + \lambda(\vec{\phi}^2)^2. \tag{3.13}$$

Let us consider the action

$$S = \frac{1}{f}\int \mathrm{d}^D x \partial_\mu\vec{\phi}\partial_\mu\vec{\phi} + \alpha(\vec{\phi}^2 - 1)^2, \tag{3.14}$$

which reduces to the non–linear sigma model by taking the $\alpha \to \infty$ limit. Rescaling the ϕ field as $\phi \to \sqrt{f}\phi$, we get

$$S = \int \mathrm{d}^D x \partial_\mu\vec{\phi}\partial_\mu\vec{\phi} + \alpha(f\vec{\phi}\cdot\vec{\phi} - 1)^2, \tag{3.15}$$

from which we can obtain the parameters of ϕ^4 theory that reproduce the non–linear sigma model as,

$$\begin{aligned} \lambda &= \alpha f^2 \\ m^2 &= -2\alpha f. \end{aligned} \tag{3.16}$$

Thus we can interpret the non–linear sigma model as a renormalizable theory in a special limit of the coupling constants. Expecting that the universality of ϕ^4 theory holds also for such a limiting case, it is natural that we should obtain the same critical phenomenon.

In the case of quantum Einstein gravity, the non–linearity of the system is not such a fictitious one and it seems difficult to find some renormalizable theory which reproduce Einstein gravity in a special limit. However, the example of the non–linear sigma model shows at least that perturbative arguments may sometimes fail concerning the existence of a non–trivial theory when the fixed–point coupling constant is not sufficiently small. Thus we need a non–perturbative study to make a definite conclusion as to whether we can construct a consistent quantum theory of Einstein gravity in dimensions greater than two.

3.2 ϵ–expansion around two dimensions

When we consider $D = 2 + \epsilon$ dimensions, the fixed–point coupling is $O(\epsilon)$ if it exists at all. Then the perturbative expansion with respect to the coupling constant is turned into the ϵ–expansion. If the convergence radius is sufficiently large, this provides a systematic approximation to higher–dimensional quantum gravity. This method is successful in the case of non–linear sigma model and it is known to give critical exponents consistent with numerical simulations of the three–dimensional

model. Although the attempts to apply this method to quantum gravity was initiated more than ten years ago [21], it is quite recently that the essential problems in the formalism have been clarified [22, 23, 24]. The application also extends to interesting problems in two–dimensional quantum gravity [25, 26, 27]. Let us here have a brief look at recent progress in $(2+\epsilon)$–dimensional quantum gravity [28, 29], for it provides us with a qualitative understanding of higher–dimensional quantum gravity.

3.2.1 The model

We consider Einstein gravity with c copies of scalar fields coupled in the conformally invariant way, which is described by the following action.

$$\begin{aligned} S &= S_G + S_M, \\ S_G &= \frac{\mu^\epsilon}{G}\int \mathrm{d}^D x\sqrt{g}R, \\ S_M &= \frac{\mu^\epsilon}{G}\int \mathrm{d}^D x\sqrt{g}\left\{\frac{1}{2}g^{\mu\nu}\partial_\mu\varphi_i\partial_\nu\varphi_i - R\frac{\epsilon}{8(D-1)}\varphi_i^2\right\}. \end{aligned} \tag{3.17}$$

The index i runs from 1 to c. Let us parametrize the metric as

$$g_{\mu\nu} = \tilde{g}_{\mu\nu}\mathrm{e}^{-\phi} = \hat{g}_{\mu\rho}(\mathrm{e}^h)^\rho{}_\nu \mathrm{e}^{-\phi}, \tag{3.18}$$

where $h^\mu{}_\nu$ is the traceless symmetric tensor. We have introduced the background metric $\hat{g}_{\mu\nu}$ for later convenience. Using the above decomposition, we get,

$$\begin{aligned} S_G &= \frac{\mu^\epsilon}{G}\int \mathrm{d}^D x\sqrt{\hat{g}}\mathrm{e}^{-\frac{\epsilon}{2}\phi}\left\{\tilde{R} - \frac{\epsilon(D-1)}{4}\tilde{g}^{\mu\nu}\partial_\mu\phi\partial_\nu\phi\right\} + \text{total derivative} \\ S_M &= \frac{\mu^\epsilon}{G}\int \mathrm{d}^D x\sqrt{\hat{g}}\left\{\frac{1}{2}\tilde{g}^{\mu\nu}\partial_\mu(\varphi_i\mathrm{e}^{-\frac{\epsilon}{4}\phi})\partial_\nu(\varphi_i\mathrm{e}^{-\frac{\epsilon}{4}\phi}) - \tilde{R}\frac{\epsilon}{8(D-1)}(\varphi_i\mathrm{e}^{-\frac{\epsilon}{4}\phi})^2\right\}. \end{aligned}$$

Redefining the matter field as

$$\varphi_i \longrightarrow \mathrm{e}^{\frac{\epsilon}{4}\phi}\varphi_i, \tag{3.19}$$

we obtain the following action

$$\begin{aligned} S = \frac{\mu^\epsilon}{G}\int \mathrm{d}^D x\sqrt{\hat{g}}\Bigg[&\mathrm{e}^{-\frac{\epsilon}{2}\phi}\left\{\tilde{R} - \frac{\epsilon(D-1)}{4}\tilde{g}^{\mu\nu}\partial_\mu\phi\partial_\nu\phi\right\} \\ &+ \left\{\frac{1}{2}\tilde{g}^{\mu\nu}\partial_\mu\varphi_i\partial_\nu\varphi_i - \tilde{R}\frac{\epsilon}{8(D-1)}\varphi_i^2\right\}\Bigg]. \end{aligned} \tag{3.20}$$

One can see that the conformal mode decouples from the matter, which is a result of the conformally invariant coupling we have chosen. Due to this fact, we can further simplify the theory by redefining the conformal mode as

$$\mathrm{e}^{-\frac{\epsilon}{4}\phi} = \sqrt{\frac{\epsilon}{8(D-1)}}\psi, \tag{3.21}$$

which makes the action

$$\begin{aligned} S = \frac{\mu^\epsilon}{G}\int \mathrm{d}^D x\sqrt{\hat{g}}\Bigg\{&\tilde{R}\frac{\epsilon}{8(D-1)}\psi^2 - \frac{1}{2}\tilde{g}^{\mu\nu}\partial_\mu\psi\partial_\nu\psi \\ &-\tilde{R}\frac{\epsilon}{8(D-1)}\varphi_i^2 + \frac{1}{2}\tilde{g}^{\mu\nu}\partial_\mu\varphi_i\partial_\nu\varphi_i\Bigg\}. \end{aligned} \tag{3.22}$$

Here the ψ field appears in the same way as the matter fields except for the overall minus sign. The dynamics of the conformal mode, therefore, becomes quite transparent, as compared with the original formalism (3.20), where one encounters the so–called oversubtraction problem [23, 24]. Note also that the region of $\phi \in (-\infty, \infty)$ corresponds to the region of $\psi \in [0, \infty)$. In the weak coupling regime, ϕ fluctuates around $\phi \sim 0$, which corresponds to $\psi \sim \sqrt{\frac{8(D-1)}{\epsilon}}$. Let us extend the region of ψ to $(-\infty, \infty)$, The theory (3.22), then, possesses the Z_2 symmetry $\psi \to -\psi$, which is spontaneously broken in the weak coupling regime. So long as the coupling constant is small, the theory (3.22) with $\psi \in (-\infty, \infty)$ is almost equivalent to (3.20), since the fluctuation of ψ around the nonzero expectation value is small. However, in the strong coupling regime, there is a substantial difference. In the theory (3.22), we may naturally expect that the Z_2 symmetry is restored and ψ fluctuates around $\psi \sim 0$. This is hard to consider in the original theory (3.20) since such a point corresponds to $\phi \sim \infty$. From this point of view, the theory (3.22) seems to be more natural than the original one (3.20).

3.2.2 General covariance and the anomaly

Let us consider the general covariance of the theory. The action (3.17) is invariant under the diffeomorphism

$$\delta g_{\mu\nu} = \partial_\mu\epsilon^\rho g_{\rho\nu} + g_{\mu\rho}\partial_\nu\epsilon^\rho + \epsilon^\rho\partial_\rho g_{\mu\nu}. \tag{3.23}$$

Let us translate this into the transformations of $\tilde{g}_{\mu\nu}$ and ψ. For simplicity, we set $\hat{g}_{\mu\nu} = \delta_{\mu\nu}$ here. Then $\tilde{g}_{\mu\nu}$ and ψ can be given in terms of $g_{\mu\nu}$ as,

$$\tilde{g}_{\mu\nu} = \frac{1}{(\det g)^{\frac{1}{D}}} g_{\mu\nu} \tag{3.24}$$

$$\psi = \sqrt{\frac{8(D-1)}{\epsilon}}(\det g)^{\frac{\epsilon}{4D}}, \tag{3.25}$$

which give the corresponding transformation for each. The transformation of the matter fields can be chosen so that the action is kept invariant. The symmetry of the tree–level action is, thus, given by

$$\begin{aligned}
\delta\tilde{g}_{\mu\nu} &= \partial_\mu\epsilon^\rho\tilde{g}_{\rho\nu} + \tilde{g}_{\mu\rho}\partial_\nu\epsilon^\rho + \epsilon^\rho\partial_\rho\tilde{g}_{\mu\nu} - \frac{2}{D}\partial_\rho\epsilon^\rho\tilde{g}_{\mu\nu}, \\
\delta\psi &= \epsilon^\rho\partial_\rho\psi + \frac{\epsilon}{2D}\psi\partial_\rho\epsilon^\rho, \\
\delta\varphi_i &= \epsilon^\rho\partial_\rho\varphi_i + \frac{\epsilon}{2D}\varphi_i\partial_\rho\epsilon^\rho.
\end{aligned} \tag{3.26}$$

Let us next consider the one–loop renormalization of the theory. As is explained earlier, we consider a perturbation around the nonzero vacuum expectation value of the ψ–field $\sqrt{\frac{8(D-1)}{\epsilon}}$. We, therefore, shift the ψ–field as

$$\psi \longrightarrow \sqrt{\frac{8(D-1)}{\epsilon}} + \psi, \tag{3.27}$$

in (3.22), and then expand around $\psi \sim 0$. Thus we arrive at the following action

$$\begin{aligned}
S = \frac{\mu^\epsilon}{G}\int \mathrm{d}^D x\sqrt{\tilde{g}}\Bigg[\tilde{R}\left\{\left(1+\sqrt{\frac{\epsilon}{8(D-1)}}\psi\right)^2 - \frac{\epsilon}{8(D-1)}\varphi_i^2\right\} \\
-\frac{1}{2}\tilde{g}^{\mu\nu}\partial_\mu\psi\partial_\nu\psi + \frac{1}{2}\tilde{g}^{\mu\nu}\partial_\mu\varphi_i\partial_\nu\varphi_i\Bigg].
\end{aligned} \tag{3.28}$$

One can see from this action that the one–loop matter contribution gives rise to the divergence of the form $\sim \frac{1}{\epsilon}\int \mathrm{d}^D x\sqrt{\tilde{g}}\tilde{R}$. Therefore the one–loop counterterm cannot be taken to be invariant under the transformation (3.26). This can be viewed as a manifestation of the conformal anomaly with respect to the conformal transformation of the background metric. This problem is, therefore, inevitable as long as we respect the general covariance of the tree–level action. Note that this kind

of thing does not occur in ordinary gauge theories, since it is deeply rooted in the nature of quantum gravity where the gauge invariance is related to changing the scale of the system locally.

Let us, then, consider generalizing the tree–level action. Here, one should note that the one–loop divergence is invariant under the transformation (3.26) for such ϵ^ρ that satisfies $\partial_\rho\epsilon^\rho = 0$, which can be called "volume–preserving diffeomorphism". Thus, we are lead to consider the most general action that is invariant under the volume–preserving diffeomorphism,

$$S = \frac{\mu^\epsilon}{G}\int \mathrm{d}^D x\sqrt{\tilde{g}}\left\{\tilde{R}L(\psi,\varphi_i) - \frac{1}{2}\tilde{g}^{\mu\nu}\partial_\mu\psi\partial_\nu\psi + \frac{1}{2}\tilde{g}^{\mu\nu}\partial_\mu\varphi_i\partial_\nu\varphi_i\right\}, \tag{3.29}$$

where $L(\psi,\varphi_i)$ is a function of ψ and φ_i with the constraint $L(0,0) = 1$. Note that the original action (3.28) corresponds to

$$L(\psi,\varphi_i) = 1 + \sqrt{\frac{\epsilon}{2(D-1)}}\psi + \frac{\epsilon}{8(D-1)}(\psi^2 - \varphi_i^2). \tag{3.30}$$

Let us consider a transformation which is the counterpart of diffeomorphism in the generalized theory. We consider a transformation,

$$\begin{aligned}
\delta\tilde{g}_{\mu\nu} &= \partial_\mu\epsilon^\rho\tilde{g}_{\rho\nu} + \tilde{g}_{\mu\rho}\partial_\nu\epsilon^\rho + \epsilon^\rho\partial_\rho\tilde{g}_{\mu\nu} - \delta\rho\tilde{g}_{\mu\nu}, \\
\delta\psi &= \epsilon^\rho\partial_\rho\psi + \mathcal{A}\delta\rho, \\
\delta\varphi_i &= \epsilon^\rho\partial_\rho\varphi_i + \mathcal{B}\delta\rho,
\end{aligned} \tag{3.31}$$

where $\delta\rho = \frac{2}{D}\partial_\rho\epsilon^\rho$. $\mathcal{A}$ and $\mathcal{B}$ will be fixed later. The action transforms as

$$\begin{aligned}
\delta S = \int \mathrm{d}^D x\sqrt{\tilde{g}}\Bigg[\left\{-\frac{\epsilon}{2}\tilde{R}\delta\rho - (D-1)\tilde{g}^{\mu\nu}\tilde{\nabla}_\mu\partial_\nu\delta\rho\right\}L \\
+\tilde{R}\frac{\partial L}{\partial\psi}\mathcal{A}\delta\rho + \frac{\epsilon}{4}\partial_\mu\psi\partial_\nu\psi\tilde{g}^{\mu\nu}\delta\rho - \tilde{g}^{\mu\nu}\partial_\mu\psi\partial_\nu(\mathcal{A}\delta\rho) \\
+\tilde{R}\frac{\partial L}{\partial\varphi_i}\mathcal{B}\delta\rho - \frac{\epsilon}{4}\partial_\mu\varphi_i\partial_\nu\varphi_i\tilde{g}^{\mu\nu}\delta\rho + \tilde{g}^{\mu\nu}\partial_\mu\varphi_i\partial_\nu(\mathcal{B}\delta\rho)\Bigg]
\end{aligned} \tag{3.32}$$

Through partial integration, one gets,

$$\delta S = \int \mathrm{d}^D x\sqrt{\tilde{g}}\left\{-\frac{\epsilon}{2}\tilde{R}L - (D-1)\tilde{g}^{\mu\nu}\tilde{\nabla}_\mu\partial_\nu L\right.$$

$$+\tilde{R}\frac{\partial L}{\partial\psi}\mathcal{A}+\frac{\epsilon}{4}\tilde{g}^{\mu\nu}\partial_\mu\psi\partial_\nu\psi+\tilde{g}^{\mu\nu}\tilde{\nabla}_\mu\partial_\nu\psi\mathcal{A}$$
$$+\tilde{R}\frac{\partial L}{\partial\varphi_i}\mathcal{B}-\frac{\epsilon}{4}\tilde{g}^{\mu\nu}\partial_\mu\varphi_i\partial_\nu\varphi_i-g^{\mu\nu}\tilde{\nabla}_\mu\partial_\nu\varphi_i\mathcal{B}\Big\}\delta\rho. \qquad (3.33)$$

The $\tilde{g}^{\mu\nu}\tilde{\nabla}_\mu\partial_\nu L$ in the first line of the above expression is given by

$$\begin{aligned}\tilde{g}^{\mu\nu}\tilde{\nabla}_\mu\partial_\nu L &= \tilde{g}^{\mu\nu}\tilde{\nabla}_\mu\left(\frac{\partial L}{\partial\psi}\partial_\nu\psi+\frac{\partial L}{\partial\varphi_i}\partial_\nu\varphi_i\right)\\ &= \tilde{g}^{\mu\nu}\left(\frac{\partial^2 L}{\partial\psi^2}\partial_\mu\psi\partial_\nu\psi+\frac{\partial L}{\partial\psi}\tilde{\nabla}_\mu\partial_\nu\psi\right.\\ &\quad\left.+\frac{\partial^2 L}{\partial\varphi_i^2}\partial_\mu\varphi_i\partial_\nu\varphi_i+\frac{\partial L}{\partial\varphi_i}\tilde{\nabla}_\mu\partial_\nu\varphi_i\right). \qquad (3.34)\end{aligned}$$

In order to get rid of $\tilde{g}^{\mu\nu}\tilde{\nabla}_\mu\partial_\nu\psi$ and $\tilde{g}^{\mu\nu}\tilde{\nabla}_\mu\partial_\nu\varphi_i$ in δS, we have to choose $\mathcal{A}$ and $\mathcal{B}$ as

$$\mathcal{A} = (D-1)\frac{\partial L}{\partial\psi} \qquad (3.35)$$
$$\mathcal{B} = -(D-1)\frac{\partial L}{\partial\varphi_i}. \qquad (3.36)$$

Let us, therefore, consider the following transformation as the counterpart of diffeomorphism in the generalized theory.

$$\begin{aligned}\delta\tilde{g}_{\mu\nu} &= \partial_\mu\epsilon^\rho\tilde{g}_{\rho\nu}+\tilde{g}_{\mu\rho}\partial_\nu\epsilon^\rho+\epsilon^\rho\partial_\rho\tilde{g}_{\mu\nu}-\frac{2}{D}\partial_\rho\epsilon^\rho\tilde{g}_{\mu\nu},\\ \delta\psi &= \epsilon^\rho\partial_\rho\psi+(D-1)\frac{\partial L}{\partial\psi}\frac{2}{D}\partial_\rho\epsilon^\rho,\\ \delta\varphi_i &= \epsilon^\rho\partial_\rho\varphi_i-(D-1)\frac{\partial L}{\partial\varphi_i}\frac{2}{D}\partial_\rho\epsilon^\rho. \qquad (3.37)\end{aligned}$$

If L is given by (3.30), this reduces to the ordinary diffeomorphism (3.26).

The change of the action under the above transformation can be obtained as

$$\begin{aligned}\delta S &= \frac{\mu^\epsilon}{G}\int \mathrm{d}^D x\sqrt{\tilde{g}}\left[\frac{1}{2}\left\{\epsilon L-2(D-1)\left(\left(\frac{\partial L}{\partial\psi}\right)^2-\left(\frac{\partial L}{\partial\varphi_i}\right)^2\right)\right\}\tilde{R}\right.\\ &\quad-\frac{1}{4}\left\{\epsilon-4(D-1)\frac{\partial^2 L}{\partial\psi^2}\right\}\partial_\mu\psi\partial_\nu\psi\tilde{g}^{\mu\nu}\\ &\quad\left.+\frac{1}{4}\left\{\epsilon+4(D-1)\frac{\partial^2 L}{\partial\varphi_i^2}\right\}\partial_\mu\varphi_i\partial_\nu\varphi_i\tilde{g}^{\mu\nu}\right]\delta\rho. \qquad (3.38)\end{aligned}$$

One can check that this vanishes if we substitute L with (3.30).

With proper gauge fixing and using the background field method, the one–loop divergence of this theory is evaluated to be [28]

$$\int \mathrm{d}^D x\sqrt{\tilde{g}}\left\{\frac{26-(1+c)}{24\pi\epsilon}\right\}\tilde{R}. \qquad (3.39)$$

Hence the one loop bare action is

$$S_0=\int \mathrm{d}^D x\sqrt{\tilde{g}}\frac{\mu^\epsilon}{G}\left\{\tilde{R}L(\psi,\varphi_i)-\frac{1}{2}\partial_\mu\psi\partial_\nu\psi\tilde{g}^{\mu\nu}+\frac{1}{2}\partial_\mu\varphi_i\partial_\nu\varphi_i\tilde{g}^{\mu\nu}-\frac{A}{\epsilon}G\tilde{R}\right\}, \qquad (3.40)$$

where $A=\frac{25-c}{24\pi}$.

3.2.3 Renormalization group trajectory and the general covariance

Let us next examine the renormalization of the coupling constants. We define the bare quantities through

$$\frac{1}{G_0} = \frac{\mu^\epsilon}{G}\left(1-\frac{AG}{\epsilon}\right), \qquad (3.41)$$
$$\frac{1}{G_0}\partial_\mu\psi_0\partial^\mu\psi_0 = \frac{\mu^\epsilon}{G}\partial_\mu\psi\partial^\mu\psi, \qquad (3.42)$$
$$\frac{1}{G_0}\partial_\mu\varphi_0^i\partial^\mu\varphi_0^i = \frac{\mu^\epsilon}{G}\partial_\mu\varphi^i\partial^\mu\varphi^i, \qquad (3.43)$$
$$L_0(\psi_0,\varphi_0^i) = L(\psi,\varphi^i)-\frac{AG}{\epsilon}+\frac{AG}{\epsilon}L(\psi,\varphi^i). \qquad (3.44)$$

By solving these equations, we obtain

$$\psi_0 = \psi\left(1+\frac{AG}{2\epsilon}\right), \qquad (3.45)$$
$$\varphi_0^i = \varphi^i\left(1+\frac{AG}{2\epsilon}\right), \qquad (3.46)$$
$$\begin{aligned}L_0(\psi_0,\varphi_0^i) &= L(\psi_0,\varphi_0^i)-\frac{AG}{\epsilon}+\frac{AG}{\epsilon}L(\psi_0,\varphi_0^i)\\ &\quad-\frac{AG}{2\epsilon}\psi_0\frac{\partial L}{\partial\psi_0}-\frac{AG}{2\epsilon}\varphi_0^i\frac{\partial L}{\partial\varphi_0^i}, \qquad (3.47)\end{aligned}$$

from which we can calculate the β functions as

$$\beta_G = \epsilon G - AG^2, \tag{3.48}$$

$$\beta_L = -AG(L-1) + \frac{AG}{2}\psi\frac{\partial L}{\partial \psi} + \frac{AG}{2}\varphi^i\frac{\partial L}{\partial \varphi^i}. \tag{3.49}$$

The expression (3.49) shows that we can restrict the form of L to

$$L = 1 + a\psi + b\psi^2 - d\varphi_i^2. \tag{3.50}$$

The β functions for a, b and d can be obtained as

$$\beta_a = -\frac{AG}{2}a, \tag{3.51}$$

$$\beta_b = 0, \tag{3.52}$$

$$\beta_d = 0. \tag{3.53}$$

Let us, then, examine the renormalization group trajectory of the theory in the two dimensional coupling space of G and a. Since $A = \frac{25-c}{24\pi}$, we have the ultra–violet fixed point $G^* = \frac{\epsilon}{A}$, $a^* = 0$, so long as $c < 25$. The $G = 0$ line is the infrared fixed line on which resides the particular point that corresponds to the conformally coupled Einstein gravity. We are interested in the renormalization trajectory which flows out of the ultra–violet fixed point into the conformally coupled Einstein gravity. The important question is whether the general covariance is maintained along the renormalization group trajectory.

Under the transformation (3.37), the bare action (3.40) changes as,

$$\begin{aligned}\delta S_0 = & -\int \mathrm{d}^D x\sqrt{\tilde{g}}\frac{\mu^\epsilon}{G}\left[\frac{1}{2}\left\{\epsilon L - AG - 2(D-1)\left(\left(\frac{\partial L}{\partial\psi}\right)^2 - \left(\frac{\partial L}{\partial\varphi_i}\right)^2\right)\right\}\tilde{R}\right. \\ & -\frac{1}{4}\left\{\epsilon - 4(D-1)\frac{\partial^2 L}{\partial\psi^2}\right\}\partial_\mu\psi\partial_\nu\psi\tilde{g}_{\mu\nu} \\ & \left.+\frac{1}{4}\left\{\epsilon + 4(D-1)\frac{\partial^2 L}{\partial\varphi_j^2}\right\}\partial_\mu\varphi_i\partial_\nu\varphi_i\tilde{g}_{\mu\nu}\right]\delta\rho,\end{aligned} \tag{3.54}$$

where $\delta\rho = \frac{2}{D}\partial_\mu\epsilon^\mu$. The only difference from the tree–level expression (3.38) comes from the one–loop counterterm. Since the second and third terms in (3.54) vanish

identically, we need to consider only the first term. If we substitute L with its explicit parametrization (3.50), the coefficient of $\tilde{R}$ becomes,

$$\begin{aligned}&\frac{\mu^\epsilon}{G}\left[\{\epsilon - AG - 2(D-1)a^2\} + \{\epsilon - 8(D-1)b\}a\psi\right. \\ &\left.+\{\epsilon - 8(D-1)b\}b\psi^2 - \{\epsilon - 8(D-1)d\}d\varphi_i^2\right] \\ = \ &\frac{\mu^\epsilon}{G}\{\epsilon - AG - 2(D-1)a^2\}.\end{aligned} \tag{3.55}$$

In order to ensure the general covariance of the theory, we have to make sure that this quantity vanishes. Differentiating this quantity with respect to μ, we get

$$\begin{aligned}&\mu\frac{\partial}{\partial\mu}\left\{\frac{\mu^\epsilon}{G}(\epsilon - AG - 2(D-1)a^2)\right\} \\ = \ &\epsilon\mu^\epsilon\frac{1}{G}\{\epsilon - AG - 2(D-1)a^2\} + \mu^\epsilon\left(-\frac{1}{G}\right)\beta_G\{\epsilon - 2(D-1)a^2\} \\ &-\mu^\epsilon\frac{1}{G}2(D-1)2a\beta_a \\ = \ &\frac{\mu^\epsilon}{G}[\epsilon\{(\epsilon - AG) - 2(D-1)a^2\} - (\epsilon - AG)\{\epsilon - 2(D-1)a^2\} \\ &+2(D-1)AGa^2] \\ = \ &0,\end{aligned} \tag{3.56}$$

where we used the expressions for β functions (3.48) and (3.51). Therefore the above quantity remains constant along each renormalization group trajectory. Note here that since $G(\mu) \propto \mu^\epsilon$ when μ goes to 0, $\frac{\mu^\epsilon}{G} \to$ const. > 0 in the infrared limit. Therefore, if we choose the particular renormalization group trajectory that flows into the infrared fixed point that corresponds to the conformally coupled Einstein gravity ($G = 0$, $a = \frac{1}{\sqrt{2(D-1)}}$), the above quantity vanishes all along the trajectory, which ensures the general covariance of the theory.

3.2.4 The ultra–violet fixed point

We have found in the previous section that the short distance structure of spacetime is described by the following action in conformally coupled Einstein gravity near two dimensions.

$$\int \mathrm{d}^D x\sqrt{\tilde{g}}\frac{\mu^\epsilon}{G^*}\{\tilde{R}(1 + \frac{\epsilon}{8(D-1)}(\psi^2 - \varphi_i^2)) \tag{3.57}$$

$$-\frac{1}{2}\partial_\mu\psi\partial_\nu\psi\tilde{g}^{\mu\nu}+\frac{1}{2}\partial_\mu\varphi_i\partial_\nu\varphi_i\tilde{g}^{\mu\nu}\}. \tag{3.58}$$

One sees that it is invariant under the transformation $\psi \to -\psi$. Considering that the ψ in the above expression originally represents a fluctuation around a nonzero vacuum expectation value, the above fact can be understood as a result of the Z_2 symmetry in the original action (3.22) being restored in the ultraviolet limit due to the large fluctuation of ψ. We also comment that we can rotate ψ field into the pure–imaginary direction $\psi \to i\psi$ in the fixed–point action without violating its reality. The conformal mode, then, becomes indistinguishable from the conformally coupled matter fields. We might expect that such a theory describes the strong coupling phase of quantum gravity beyond the ultra–violet fixed point.

In order to establish the validity of the ϵ–expansion approach in quantum gravity, we have to show that the higher order corrections can be computed systematically. In Ref. [29], we examined the theory at the two–loop level. Since the two–loop calculations in quantum gravity is a formidable task due to the proliferation of diagrams and tensor indices, we have decided to calculate the two–loop counterterms which are proportional to the number of matter fields (the central charge) as a first step. Since the central charge is a free parameter, the counterterms must be of the renormalizable form. They further must satisfy the requirement from general covariance. Therefore this calculation serves as a check of the ϵ–expansion approach.

We concentrate on the short distance fixed point of the renormalization group. At the fixed point the tree action is

$$\frac{\mu^2}{G}\int \mathrm{d}^D x\sqrt{\hat{g}}\left\{\tilde{R}L(X_i)+\frac{1}{2}\tilde{g}^{\mu\nu}\partial_\mu X_i\partial_\nu X^i\right\}, \tag{3.59}$$

where $L = 1 - bX_iX^i$. X_i denotes ψ and φ_i fields ($X_0 = \psi$) and $X_iX^i = -\psi^2 + \sum_{j=1}^{c}\varphi_j{}^2$. This action possesses the Z_2 invariance $X_i \to -X_i$. We compute the counterterms at the fixed point where further simplification takes place due to the Z_2 invariance. Note that the conformal mode ψ is just another matter field at the fixed point. Therefore the conformal mode contribution can be included by the replacement $c \to c + 1$.

We have calculated the divergences proportional to the central charge and examined how the non–local terms as well as infrared divergences in the $\frac{1}{\epsilon}$ pole cancel among the diagrams. It has been shown that the ultra–violet fixed point exists which possesses the general covariance up to two–loop level in the leading order of the central charge. We have to work out similar calculations without imposing the Z_2 symmetry on the system in order to examine the general covariance on the renormalization trajectory that flows into the classical Einstein gravity. It seems also important for us to perform the full calculation of two–loop renormalization without restricting ourselves to the leading matter contribution. We hope that we can eventually calculate physical quantities such as critical exponents, which may also be calculable in numerical simulations of three or four dimensional quantum gravity in future.

3.3 Numerical simulation based on dynamical triangulation

3.3.1 Lattice action

In the previous section we have seen that the recent progress in the ϵ–expansion approach to higher–dimensional quantum gravity is quite promising. At least it seems that the ϵ–expansion can be formulated as well as in ordinary field theories, in spite of the subtleties concerning the conformal anomaly. Needless to say, this does not prove the existence of a consistent theory of quantum gravity in physical dimensions such as three or four. In order to make a definite conclusion as to this problem, a non–perturbative study is necessary. In this section, we consider numerical simulations of higher–dimensional quantum gravity based on dynamical triangulation.

In dynamical triangulation we replace the path integral over the metric with summation over all the triangulation made of equilateral D–simplices. We first

summarize the basic knowledge on simplicial manifolds.

We denote the number of p–simplices in a configuration by N_p $(p = 0, 1, \cdots, D)$. Let us also define the order of a p–simplex σ_p as the number of D–simplices sharing the simplex σ_p and denote it by $o(\sigma_p)$. Note that

$$o(\sigma_D) = 1, \tag{3.60}$$

$$o(\sigma_{D-1}) = 2. \tag{3.61}$$

Since we require the configuration to be a simplicial complex in the strictly mathematical sense, each D–simplex should face to different $(D+1)$ D–simplices. Therefore we have,

$$o(\sigma_p) \geq D + 1 - p \qquad \text{for} \quad p \leq D - 2. \tag{3.62}$$

Also, we have the following relation

$$\sum_{\sigma_p} o(\sigma_p) = \begin{pmatrix} D+1 \\ p+1 \end{pmatrix} N_D, \tag{3.63}$$

which comes from the fact that a D–simplex contains ${}_{D+1}\mathrm{C}_{p+1}$ p–simplices.

There are relations among N_p's. Since each $(D-1)$–simplex is shared by two D–simplices (eq. (3.61)) and each D–simplex contains $(D+1)$ $(D-1)$–simplices (eq. (3.63) for $p = D-1$), we have

$$2N_{D-1} = (D+1)N_D. \tag{3.64}$$

The Euler number is defined as

$$\chi = \sum_{p=0}^{D} (-1)^p N_p, \tag{3.65}$$

which is a topologically invariant number.

We have another relation from the restriction that the configuration should satisfy the manifold condition, i.e. if we draw an infinitesimal hypersphere around a vertex, the intersection of this sphere with the manifold should be homeomorphic to S^{D-1}. In one and two dimensions this is trivially satisfied. Let us consider three–dimensional case. Let us draw an infinitesimal hypersphere around a vertex, and

consider the intersection of this sphere with the manifold. We denote the number of i–simplices in this intersection by N_i'. Then the manifold condition requires,

$$N_0' - N_1' + N_2' = 2. \tag{3.66}$$

If we sum up this equation over all the vertices in the manifold, we obtain

$$2N_1 - 3N_2 + 4N_3 = 2N_0. \tag{3.67}$$

Combining this with eq. (3.64) namely $2N_2 = 4N_3$, we get $\chi = 0$, which means that the Euler number of three–dimensional closed manifold is 0 irrespective of its topology.

Let us next consider four–dimensional case. Let us define N_i' similarly. In this case, the intersection is a three–dimensional manifold and it is difficult to impose that it is homeomorphic to S^3. However, as a necessary condition, we have

$$N_0' - N_1' + N_2' - N_3' = 0. \tag{3.68}$$

Summing this equation over all the vertices, we obtain

$$2N_1 - 3N_2 + 4N_3 - 5N_4 = 0, \tag{3.69}$$

which gives a relation independent of the Euler's relation (3.65) for $D = 4$.

Let us summarize the relations among N_p's in each dimension. In two dimensions, there are two relations among three quantities N_0,N_1,N_2.

$$N_0 - N_1 + N_2 = \chi, \tag{3.70}$$

$$2N_1 = 3N_2, \tag{3.71}$$

where χ is the Euler number, which is related to the number of handles (genus) g through $\chi = 2(1-g)$. Therefore only one of the N_p's is independent. In three dimensions, there are two relations among four quantities N_0,N_1,N_2,N_3.

$$N_0 - N_1 + N_2 - N_3 = 0, \tag{3.72}$$

$$2N_2 = 4N_3. \tag{3.73}$$

Therefore only two of the N_p's are independent. In four dimensions, there are three relations among five quantities N_0,N_1,N_2,N_3,N_4.

$$N_0 - N_1 + N_2 - N_3 + N_4 = \chi, \tag{3.74}$$

$$2N_1 - 3N_2 + 4N_3 - 5N_4 = 0, \tag{3.75}$$

$$5N_4 = 2N_3, \tag{3.76}$$

where χ is the Euler number, which is two for S^4 topology. Therefore only two of the N_p's are independent.

Let us then consider the lattice counterpart of the Einstein–Hilbert action

$$S = \int \mathrm{d}^D x \sqrt{g}(\Lambda - \frac{1}{G}R). \tag{3.77}$$

The cosmological term can be naturally identified with the number of D–simplices. The lattice counterpart of the Einstein term can be derived as follows. First of all, note that the curvature is localized on $(D-2)$–simplices. Since the angle between two $(D-1)$–dimensional faces of a D–simplex is $\alpha = \arccos\frac{1}{D}$, the deficit angle around a $(D-2)$–simplex σ_{D-2} is $2\pi - \alpha o(\sigma_{D-2})$. Therefore, the lattice counterpart of the Einstein term can be obtained as follows.

$$\begin{aligned}\int \mathrm{d}^D x \sqrt{g} R \quad &\longleftrightarrow \quad \sum_{\sigma_{D-2}} \{2\pi - \alpha\, o(\sigma_{D-2})\} \\ &= 2\pi N_{D-2} - \alpha \frac{(D+1)D}{2} N_D.\end{aligned} \tag{3.78}$$

In two dimensions, we get

$$\begin{aligned}\int \mathrm{d}^2 x \sqrt{g} R &= 2\pi(N_0 - \frac{1}{2}N_2) \\ &= 2\pi\chi,\end{aligned} \tag{3.79}$$

as expected. Thus it turns out that the number of the relevant coupling constants in the Einstein–Hilbert action is equal to the number of the independent variables in the N_p's up to four dimensions. In this sense, the Einstein–Hilbert action gives the most general lattice action that can be written as a linear combination of N_p's.

The parametrization of the lattice action is dependent on references. We quote in the following the one used by Ambjørn et al. [33, 35]. In three dimensions, one can parametrize the action as

$$S_{\mathrm{lat}} = \kappa_3 N_3 - \kappa_1 N_1. \tag{3.80}$$

κ_3 and κ_1 corresponds to the parameters in the Einstein–Hilbert action through

$$\kappa_3 = \Lambda - \frac{2\pi}{G}, \tag{3.81}$$

$$\kappa_2 = \frac{6\alpha}{G}, \tag{3.82}$$

where $\alpha = \arccos\frac{1}{3}$.

In four dimensions, one can parametrize the action as

$$S_{\mathrm{lat}} = \kappa_4 N_4 - \kappa_2 N_2. \tag{3.83}$$

κ_4 and κ_2 corresponds to the parameters in the Einstein–Hilbert action through

$$\kappa_4 = \Lambda - \frac{2\pi}{G}, \tag{3.84}$$

$$\kappa_2 = \frac{10\alpha}{G}, \tag{3.85}$$

where $\alpha = \arccos\frac{1}{4}$.

Although in continuum theory, the number of operators are restricted due to the general covariance, there are a lot of degrees of freedom in the operator on a lattice. In this section we have considered the lattice counterpart of the Einstein–Hilbert action. What if we add some general local terms written in terms of $o(\sigma)$ in the action? Since general covariance is not manifest at the lattice level, and it is something that we expect to appear in the continuum limit, it is natural for us to expect that when we add general local terms to the action, general covariance will appear so long as we can obtain a sensible continuum limit. In other words, studying only the type of action derived in this section is not sufficient when we search for a non–trivial fixed point where a sensible continuum limit can be taken. Although we consider the simplest action as a first trial, we should bear in mind that we have to try various local actions, even if we fail with the simplest one.

3.3.2 Ergodic moves

In order to perform a Monte Carlo simulation to generate an ensemble, we have to define a transition probability from one configuration to another. In dynamical triangulation, we make use of a set of local changes of the triangulation called "move", which can be obtained as follows. Consider a $(D+1)$–simplex, which is made of $(D+2)$ D–simplices. Pick up an i–simplex σ_i $(i = 0, 1, \cdots, D)$ that belongs to the $(D+1)$–simplex and consider all the D–simplices sharing it. One finds that there are $(D+1-i)$ of them. Then we can define a move which replace the above $(D+1-i)$ D–simplices with the remaining $(1+i)$ D–simplices. We call it (p,q)–move, where $p = D+1-i$ and $q = 1+i$. p and q satisfy $p+q = D+2$ by definition. Note that when $p \neq q$, (q,p)–move is nothing but the inverse of (p,q)–move. In even dimensions (D=even), we have a move such that $p = q$. As is obvious from the above construction, these moves do not change the topology of the manifold. Also, the updated configuration is guaranteed to satisfy the manifold condition, so long as the old one satisfies it. This can be seen as follows. Draw an infinitesimal hypersphere around each vertex and consider the intersection of the hypersphere and the manifold. When a move is operated to the manifold, the intersection also changes according to a move in $D-1$–dimensions. Therefore, the topology of the intersection remains unchanged, which means that the manifold condition remains true, if the initial configuration satisfies it.

We illustrate the (p,q)–moves in each dimension in Figure 1.

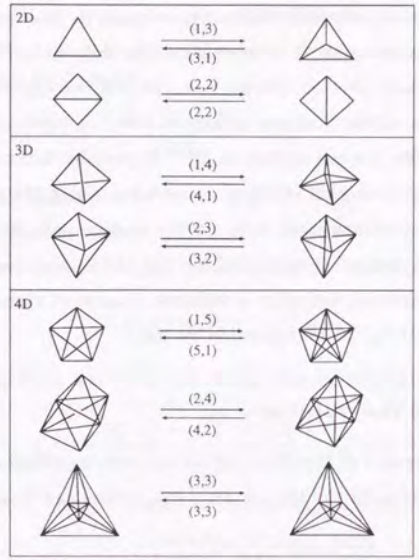

Figure 1: (p,q)-moves for two, three and four dimensions.

In order to use these moves in generating ensembles, we have to check the ergodicity. Ergodicity means that we can change an arbitrary triangulation into another arbitrary triangulation with use of finite times of moves. Ergodicity of this set of moves has been proved up to four dimensions in Ref. [30]. Actually in two dimensions, ergodicity can be shown using only (2,2)–move, as was proved quite a long time ago [31]. This enables us to simulate the two–dimensional system with fixed N_2.

When we perform a (p,q)–move, we may obtain a simplicial manifold which does not satisfy the conditions of simplicial complex. We have to reject the move and try another one in such a case. One can show that we have only to check that the new $(p-1)$–simplex which is shared by the new q D–simplices does not share all its

vertices with another $(p-1)$–simplex which already exists in the configuration.

As for the initial configuration, it is conventional to take the surface of a $(D+1)$–simplex, which contains $(D+2)$ D–simplices. In [39], we also tried an initial configuration which has almost uniform structure. Such a configuration can be constructed as follows. We use the surface of L^{D+1} hypercubic lattice. Take one of its diagonals and project it to each of the 2^{D+1} surfaces. Using the projected line, we can subdivide each D–dimensional cube on the surfaces into $D!$ D–simplices. Thus we can construct a configuration with $2(D+1)L^D D!$ D–simplices with almost uniform structure. We checked that after a sufficient number of updates, the result does not depend on which initial configuration we use.

3.3.3 Control of the volume

Using the lattice counterpart of the Einstein–Hilbert action considered in Section 3.3.1, the partition function for the four–dimensional system can be defined as

$$Z(\kappa_2, \kappa_4) = \sum_T \mathrm{e}^{-S_{\mathrm{lat}}(\kappa_2, \kappa_4)}, \tag{3.86}$$

where summation is performed over all the closed simplicial manifold with S^4 topology. This system gives a grand canonical ensemble in the sense that the size of the system is allowed to fluctuate. However, this system is not stable with respect to κ_4, namely if we take κ_4 large, N_4 keeps on decreasing, and if we take κ_4 small, N_4 keeps on increasing. This is not necessarily a problem, though, as we explain in the following. Let us consider an ensemble with a fixed total volume described by the following partition function

$$Z(\kappa_2, N_4) = \sum_{T \in \mathcal{T}_{N_4}} \mathrm{e}^{\kappa_2 N_2}, \tag{3.87}$$

where $\mathcal{T}_{N_4}$ denotes the set of closed simplicial manifolds with N_4 4–simplices. This can be referred to as a canonical ensemble, since we fix the system size. $Z(\kappa_2, \kappa_4)$ can be written by Laplace transformation of $Z(\kappa_2, N_4)$ as

$$Z(\kappa_2, \kappa_4) = \sum_{N_4} Z(\kappa_2, N_4) \mathrm{e}^{-\kappa_4 N_4} \tag{3.88}$$

$$= \sum_{N_4} \mathrm{e}^{-\kappa_4 N_4 + \ln Z(\kappa_2, N_4)}. \tag{3.89}$$

The saddle point will be given by

$$\frac{\partial \ln Z(\kappa_2, N_4)}{\partial N_4} = \kappa_4. \tag{3.90}$$

Let us denote the left hand side by ${\kappa_4}^c(\kappa_2, N_4)$. If $\frac{\partial {\kappa_4}^c(\kappa_2, N_4)}{\partial N_4} < 0$, this saddle point is stable, and otherwise unstable.

In the case of two dimensions, the partition function can be given as

$$Z(N) \sim N^{\gamma_{\mathrm{str}} - 3} \mathrm{e}^{\kappa N}, \tag{3.91}$$

for sufficiently large N, where γ_{str} is the string susceptibility given by

$$\gamma_{\mathrm{str}} = -\frac{25 - c + \sqrt{(1-c)(25-c)}}{24}\chi + 2. \tag{3.92}$$

χ is the Euler number which is related to the genus g through

$$\chi = 2(1-g). \tag{3.93}$$

For pure gravity ($c = 0$), we have

$$\gamma_{\mathrm{str}} = -\frac{5}{4}\chi + 2. \tag{3.94}$$

Since

$$\kappa^c(N) = \frac{\partial \ln Z(N)}{\partial N} = \kappa - \left\{\frac{5}{2}(1-g) + 1\right\}\frac{1}{N}, \tag{3.95}$$

the saddle point is unstable for $g = 0$ (sphere) and $g = 1$ (torus). This is not a problem, though, since we can define an ensemble average in the thermodynamic limit by differentiating with respect to the cosmological constant κ (which corresponds to inserting the cosmological term) sufficiently many times, and then take the limit $\kappa \to \kappa^c = \lim_{N\to\infty} \kappa^c(N)$. Similarly, in the case of four dimensions, the instability with respect to κ_4 is not itself a problem. If $\lim_{N_4\to\infty} {\kappa_4}^c(\kappa_2, N_4)$ diverges, however, we cannot define any sensible ensemble average from the partition function $Z(\kappa_2, \kappa_4)$, which is obviously a disaster. As we explain later, the system defined

through (3.87) has a phase transition at $\kappa_2 = \kappa_2{}^c$. When $\kappa_2 > \kappa_2{}^c$ the convergence of $\kappa_4{}^c(\kappa_2, N_4)$ is very fast and there is no problem. For $\kappa_2 < \kappa_2{}^c$, on the other hand, the convergence is very slow, and the data show a large size dependence. This problem has been addressed by many groups recently [37], and it seems that the largest–size simulation favors the existence of $\lim_{N_4\to\infty} \kappa_4{}^c(\kappa_2, N_4)$. For the special case $\kappa_2 = 0$, the partition function $Z(\kappa_2 = 0, N_4)$ is nothing but the number of triangulations with N_4 4–simplices. The existence of $\lim_{N_4\to\infty} \kappa_4{}^c(\kappa_2 = 0, N_4)$ is, therefore, equivalent to the existence of the exponential bound to the number of the triangulations with N_4 4–simplices. We also comment that in three–dimensional case, the existence of $\lim_{N_3\to\infty} \kappa_3{}^c(\kappa_1, N_3)$ is numerically established [32].

Practically, we have only to work with the canonical ensemble with fixed N_4. In two dimensions, this can be done straightforwardly, since we know a set of ergodic moves which does not change the total volume. In four dimensions, we do not know such a set of ergodic moves. Therefore the best thing we can do is to add some potential with respect to N_4 so that we can stabilize the total volume during the simulation and pick up only those configurations with a fixed N_4. The potential can be chosen as one likes, but a convenient choice is

$$S = \gamma(N_4 - N_4^{(0)})^2. \tag{3.96}$$

With this additional term, eq. (3.89) becomes

$$Z(\kappa_2, \kappa_4, \gamma) = \sum_{N_4} \mathrm{e}^{-\kappa_4 N_4 + \ln Z(\kappa_2, N_4) - \gamma(N_4 - N_4^{(0)})^2}. \tag{3.97}$$

The ensemble average of N_4 can be given by the saddle point

$$\kappa_4{}^c(\kappa, \langle N_4\rangle) = \kappa_4 + 2\gamma(\langle N_4\rangle - N_0^{(0)}). \tag{3.98}$$

Using this formula, one can measure $\kappa_4{}^c(\kappa, N_4)$ through numerical simulation.

3.3.4 Second order phase transition in four dimensions

Let us next turn to the results of numerical simulation in four dimensions. A fundamental observable, which has been measured by many groups [35, 36], is the total curvature, which we denote by R_{tot},

$$R_{\mathrm{tot}} = \int \mathrm{d}^4x\sqrt{g}R = 2\pi N_2 - 10\alpha N_4. \tag{3.99}$$

Figure 2 shows our results for the expectation value of the average curvature per unit volume $\langle R_{\mathrm{tot}}\rangle/\alpha N_4$ at various κ_2's. $\alpha = \arccos\frac{1}{4}$ in the denominator is just for conventional reason.

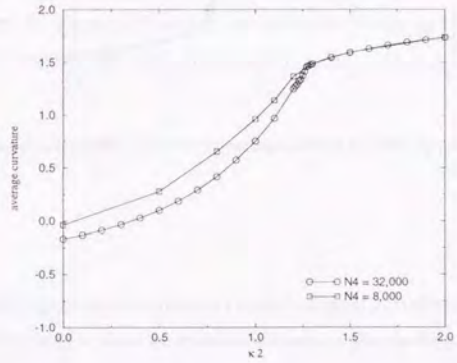

Figure 2: The average curvature per volume is plotted against κ_2 for $N_4 =$ 8000(squares) and $N_4 = 32000$(circles).

One can see that the behavior of the curve changes abruptly at $\kappa_2 = 1.2 \sim 1.3$. The susceptibility can be defined as

$$\chi = \frac{\langle R_{\mathrm{tot}}^2\rangle - \langle R_{\mathrm{tot}}\rangle^2}{\alpha N_4} \propto \frac{\partial}{\partial\kappa_2}\frac{\langle R_{\mathrm{tot}}\rangle}{\alpha N_4}. \tag{3.100}$$

We can see in Figure 3 that there is a peak in susceptibility at $\kappa_2 = 1.2 \sim 1.3$ and the height of the peak grows as the system size is increased.

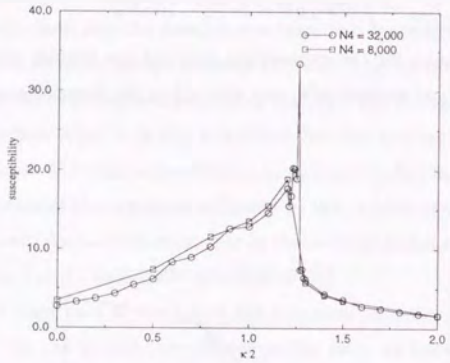

Figure 3: The susceptibility is plotted against κ_2 for $N_4 = 8000$(squares) and $N_4 = 32000$(circles).

This implies that the correlation length of local curvature is very large at the critical point, where we may hope to take a sensible continuum limit. On the other hand, in three dimensions, the average curvature shows a hysteresis as a function of the coupling constant [33]. It has been reported that this property does not change by coupling the matter fields to the system [34]. However, we remind the reader that we are allowed to put any terms in the action written in terms of local lattice variables such as $o(\sigma_p)$, on the grounds of general covariance as we mentioned in the end of Section 3.3.1.

Let us next examine the structures of configurations in detail. We first have a look at the vertex order distribution. When we decrease κ_2, the number of triangles N_2 decreases, and so does the number of vertices N_0, since both are related through

$$N_2 = 2(N_0 + N_4 - 2). \tag{3.101}$$

On the other hand, from (3.63), we have

$$\sum_v o(v) = 5N_4, \tag{3.102}$$

which means that the average vertex order $\overline{o(v)} = \sum_v o(v)/N_0 = 5N_4/N_0$ increases as κ_2 decreases. If we vary N_4 according to κ_2 so that N_0 is kept the same, we see that decreasing κ_2 amounts to adding a linear potential with a negative slope for the vertex order. In Figure 4,5 and 6, we show the vertex order distribution for $\kappa_2 = 2.0, 1.25, 0.0$ respectively with $N_4 = 32000$.

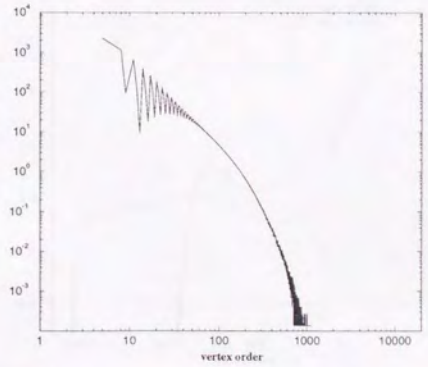

Figure 4: The vertex order distribution for $\kappa_2 = 2.0$ with $N_4 = 32000$.

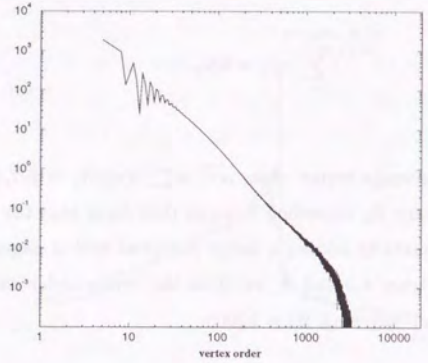

Figure 5: The vertex order distribution for $\kappa_2 = 1.25$ with $N_4 = 32000$.

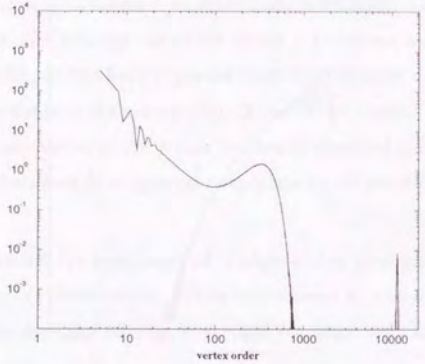

Figure 6: The vertex order distribution for $\kappa_2 = 0.0$ with $N_4 = 32000$.

One finds in Fig. 6 that there is a vertex with very large order; as large as one third of the total 4–simplices. Let us call this phenomenon as "vertex order concentration".

Vertex order is, in a sense, local connectivity of the manifold. Let us turn to the global connectivity. We consider the number of vertices $V(r)$ which are reached at r steps from a point. When $V(r)$ behaves as $\sim r^d$, we may call d the Haussdorff dimension of the manifold. Such a quantity has been measured in the second paper of Ref. [35]. As it turned out in Ref. [15], however, such a quantity is not universal at least in two–dimensional case, which warns us to be careful in considering what is the universal fractal structure in quantum gravity. Here we measure $\frac{\partial \ln V(r)}{\partial \ln r}$ in order to have a glimpse at the global connectivity of the manifold. In Figure 7, 8, and 9, we show the plot of $\frac{\partial \ln V(r)}{\partial \ln r}$ as a function of r, for κ_2 =2.0, 1.25 and 0.0 respectively with $N_4 = 8000$ and 32000.

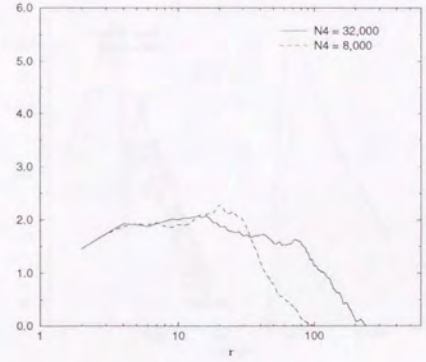

Figure 7: $\frac{\partial \ln V(r)}{\partial \ln r}$ is plotted against r for $\kappa_2 = 2.0$ with $N_4 = 8000$ (dashed line) and $N_4 = 32000$ (solid line).

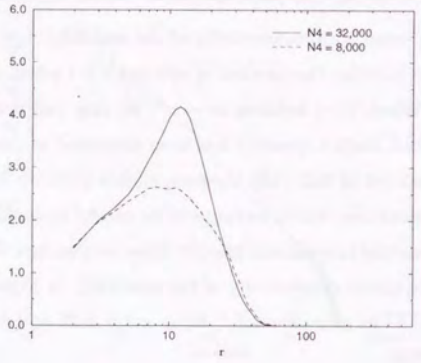

Figure 8: $\frac{\partial \ln V(r)}{\partial \ln r}$ is plotted against r for $\kappa_2 = 1.25$ with $N_4 = 8000$ (dashed line) and $N_4 = 32000$ (solid line).

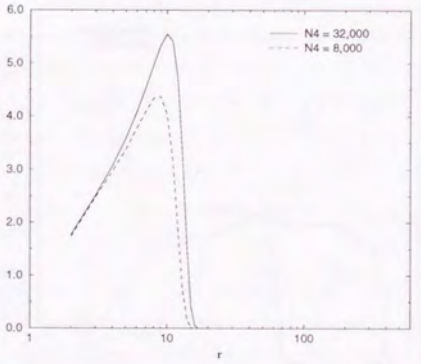

Figure 9: $\frac{\partial \ln V(r)}{\partial \ln r}$ is plotted against r for $\kappa_2 = 0.0$ with $N_4 = 8000$ (dashed line) and $N_4 = 32000$ (solid line).

One finds that at $\kappa_2 = 2.0$, the data fluctuates around two, which is substantially smaller than four. This means that the manifold cannot stretch out to make a sound four–dimensional manifold when κ_2 is large.

Another way to look at the connectivity of the configuration is to examine the pinched structure. In dynamical triangulation, we can define a minimum neck, which played a central role in the precise measurement of the string susceptibility [38]. Let us consider a lump which does not have minimum necks inside that is connected with others only through a minimum neck. Let us call the lump "baby universe" for simplicity. We measure the volume distribution of the baby universe. Figure 10, 11 and 12 show the results for κ_2 =2.0, 1.25 and 0.0 respectively with $N_4 = 8000$ and 32000.

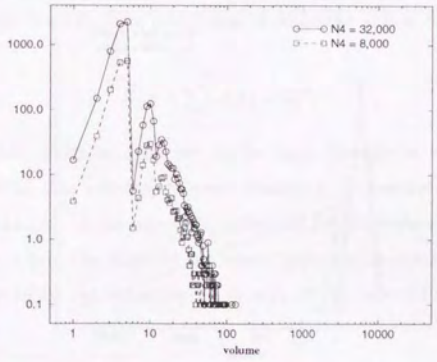

Figure 10: The volume distribution of baby universe for $\kappa_2 = 2.0$ with $N_4 = 8000$ (squares) and $N_4 = 32000$ (circles).

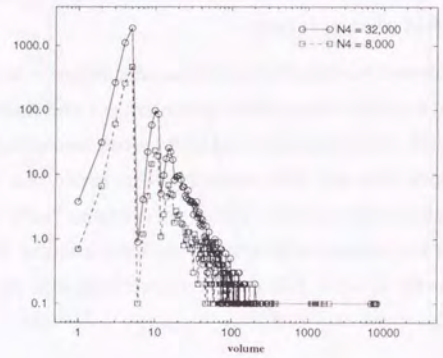

Figure 11: The volume distribution of baby universe for $\kappa_2 = 1.25$ with $N_4 = 8000$ (squares) and $N_4 = 32000$ (circles).

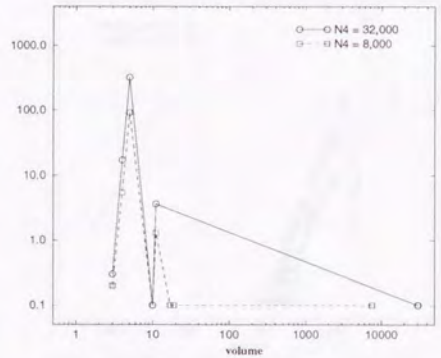

Figure 12: The volume distribution of baby universe for $\kappa_2 = 0.0$ with $N_4 = 8000$ (squares) and $N_4 = 32000$ (circles).

One finds that at $\kappa_2 = 0.0$, there is one extremely large baby universe and all the others are very small. On the other hand at $\kappa_2 = 2.0$, there is no such an extremely large baby universe. Another interesting point is that when we normalize the volume distribution of baby universe with the system size N_4, the data for $\kappa_2 = 2.0$ becomes almost identical for different N_4. This means that increasing the total volume only results in creating more baby universes with the same volume distribution. The size dependence of the average curvature per unit volume and that of Haussdorff dimension plot also support this picture. We may refer to this situation as "branched–polymer".

3.3.5 Suppression of a vertex with very large order

Let us summarize the situations for large and small κ_2 regions. In large κ_2 region, the configurations are dominated by pinched structure and the Haussdorff dimension is around two. In small κ_2 region, on the other hand, there is a large baby universe which is highly connected due to the existence of a vertex with very large order. In any case these situations are far from continuum physics. Can we have a large baby universe without vertex order concentration? In order to clarify this point, we study a theory with the following additional term in the action [1].

$$S = \lambda \sum_v \{o(v) - 5\}^2. \tag{3.103}$$

We take $\lambda = 0.005$, which is expected to be large enough to avoid vertex order concentration. With this additional term, changing κ_2 amounts to changing the position of the minimum of the parabolic potential for the vertex order, in contrast to the $\lambda = 0$ case, where the slope of the linear potential is changed. Therefore we can control $\overline{o(v)}$ without the catastrophic growth of the order of a vertex as is seen in the $\lambda = 0$ case.

[1] In Ref. [36] they studied a system with the additional term $S = -n \sum_v \ln \frac{o(v)}{5}$ with $n = -5, -1, 0, +1, +5$ in a somewhat different context. It has been reported that such a term strongly affects the criticality of the phase transition.

In Figure 13 and 14, we show the result for the average curvature per unit volume and the susceptibility respectively. We have replotted the data for $\lambda = 0$.

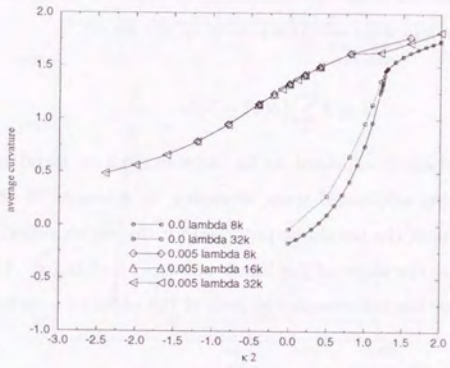

Figure 13: The average curvature per unit volume for $\lambda = 0.005$ with $N_4 = 8000, 16000, 32000$. The data for $\lambda = 0$ are also plotted.

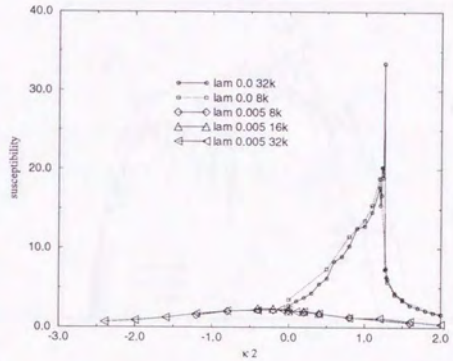

Figure 14: The susceptibility for λ =0.005 with $N_4 = 8000, 16000, 32000$. The data for $\lambda = 0$ are also plotted.

Although there is a broad peak in the susceptibility, one sees that the results seem to have no size dependence. This means that there is no phase transition and the correlation length is very small at least over the κ_2 region investigated. In Figure 15, 16 and 17, we show the data of the vertex order distribution, $\frac{\partial \ln V(r)}{\partial \ln r}$ and the volume distribution of baby universe respectively for $\kappa_2 = 0.4, -0.4$ with $\lambda = 0.005$.

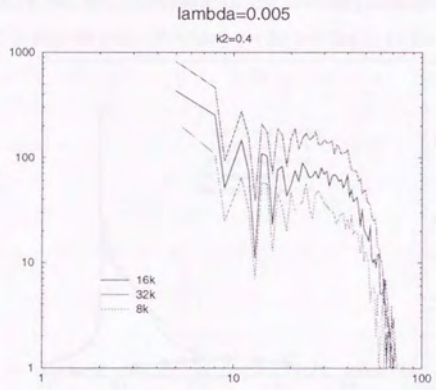

Figure 15a: The vertex order distribution for $\lambda = 0.005$, $\kappa_2 = 0.4$ with $N_4 = 8000, 16000, 32000$.

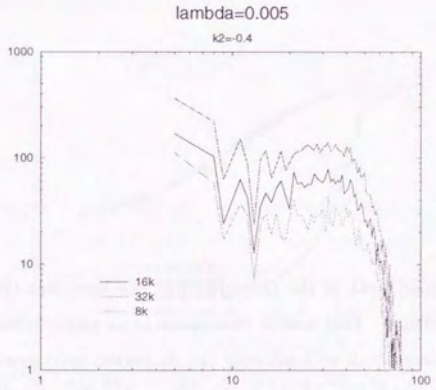

Figure 15b: The vertex order distribution for $\lambda = 0.005$, $\kappa_2 = -0.4$ with $N_4 = 8000, 16000, 32000$.

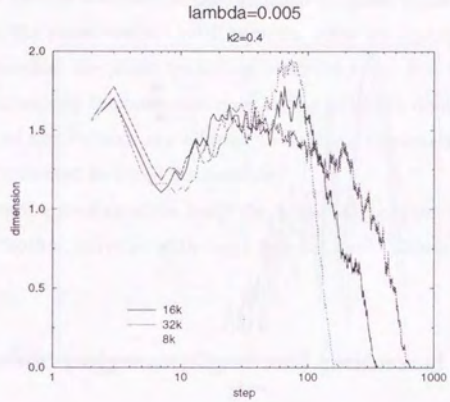

Figure 16a: $\frac{\partial \ln V(r)}{\partial \ln r}$ is plotted against r for $\lambda = 0.005$, $\kappa_2 = 0.4$ with $N_4 = 8000, 16000, 32000$.

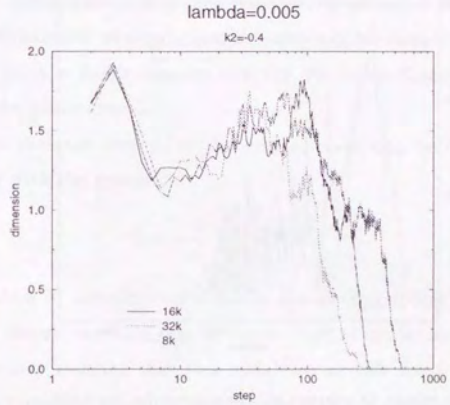

Figure 16b: $\frac{\partial \ln V(r)}{\partial \ln r}$ is plotted against r for $\lambda = 0.005$, $\kappa_2 = -0.4$ with $N_4 = 8000, 16000, 32000$.

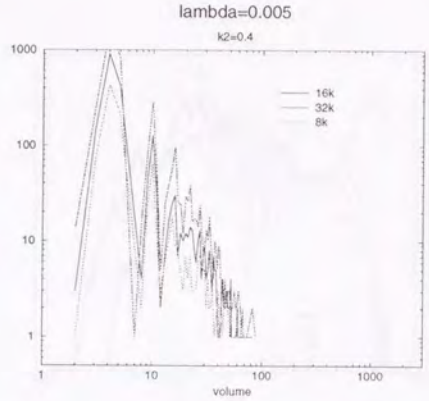

Figure 17a: The volume distribution of baby universe for $\lambda = 0.005$, $\kappa_2 = 0.4$ with $N_4 = 8000, 16000, 32000$.

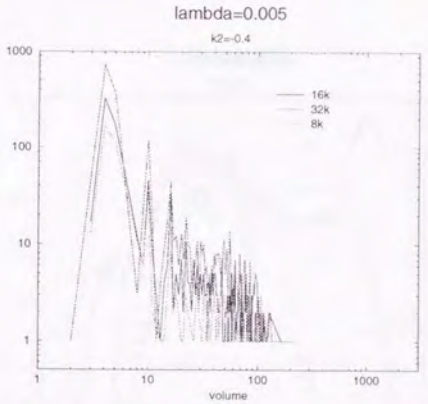

Figure 17b: The volume distribution of baby universe for $\lambda = 0.005$, $\kappa_2 = -0.4$ with $N_4 = 8000, 16000, 32000$.

All these results resembles the one for large κ_2 when $\lambda = 0$. We may therefore

conclude that the system is always in the branched–polymer phase when $\lambda = 0.005$.

The fact that the phase transition disappears when we suppress a vertex with large order implies that the phase transition observed when $\lambda = 0$ is induced by a severe competition among the baby universes trying to be the dominant one. When $\lambda = 0.005$, none of the vertices are allowed to have an extremely large order and they have to be contented in small fluctuations.

Why then does the configuration favor the branched–polymer structure instead of a single large mother universe with large fluctuations? This is the topic of the last section.

3.3.6 Branched polymer phase and conformal mode instability

The vertex order concentration is a phenomenon which can be understood as a result of the fact that the vertex order can be arbitrarily large. Although it is not trivial that such a phenomenon occurs considering the loss of entropy, at least we know how to avoid it. Understanding branched polymer, on the other hand, may not be so easy, since in dynamical triangulation, the vertex order cannot be smaller than five. The results for $\lambda = 0.005$ suggests that the smallness of each vertex order is not the cause of the phenomenon.

Let us assume that the system at the critical point can be described by the continuum theory with the action

$$S = -\frac{1}{G}\int \mathrm{d}^4x\sqrt{g}R. \tag{3.104}$$

A slight perturbation in the direction towards the weak coupling phase will eventually makes the theory unstable due to the conformal mode, as we discussed in Section 3.1. One may imagine that this instability reveals itself as the branched polymer structure. In the continuum, such an instability is necessarily related to an arbitrarily large curvature. However on a simplicial manifold, there are more degrees of freedom, so that we may have the instability even if the curvature is bounded

from above. Let us examine this possibility by measuring the conformal mode in dynamical triangulation.

Roughly speaking, the conformal mode ϕ can be identified with $\log\sqrt{g}$, as can be seen from the decomposition

$$g_{\mu\nu} = \hat{g}_{\mu\lambda}(\mathrm{e}^h)^\lambda{}_\nu \mathrm{e}^{-\phi}, \tag{3.105}$$

with the flat background metric,

$$\hat{g}_{\mu\nu} = \delta_{\mu\nu}. \tag{3.106}$$

From the relation $\sum_v o(v) = 5N_4 = \int \mathrm{d}^4x\sqrt{g}$ we can postulate the relation

$$\sqrt{g} \longleftrightarrow \log\frac{o(v)}{5}, \tag{3.107}$$

as has been done in ref. [36].

We, therefore, define the conformal mode ϕ on each vertex through

$$\phi(v) = \ln o(v). \tag{3.108}$$

We would like to know how much the conformal mode fluctuates spatially. For this purpose, we measure the correlation of the conformal mode between the nearest-neighbor vertices. We count the number of the links which has conformal mode $\phi = x$ and $\phi = y$ on either end. Let us normalize it and define the frequency $\rho(x, y)$ so that it satisfies

$$\int_{x\le y} \mathrm{d}x\mathrm{d}y\ \rho(x, y) = 1. \tag{3.109}$$

By definition, we have

$$\rho(x, y) = \rho(y, x). \tag{3.110}$$

The frequency of the link having a vertex with conformal mode $\phi = x$ on either edge can be written as

$$f(x) = \int_0^\infty \mathrm{d}y\ \rho(x, y). \tag{3.111}$$

We can define the correlation of the conformal mode between nearest neighbor vertices by

$$C(x, y) = \frac{\rho(x, y)}{f(x)f(y)}. \tag{3.112}$$

Figure 18 show the result of the correlation for $\kappa_2 = 2.0, 1.25, 0.0$ with $\lambda = 0.0$ and Figure 19 for $\kappa_2 = 0.4, 0, -0.4$ with $\lambda = 0.005$.

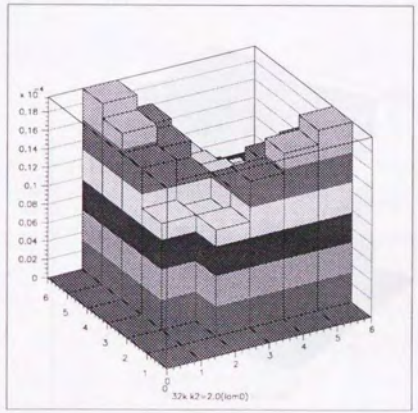

Figure 18a: The correlation $\rho(x, y)$ of the conformal mode between nearest-neighbor vertices for $\lambda = 0$, $\kappa_2 = 2.0$ with $N_4 = 32000$.

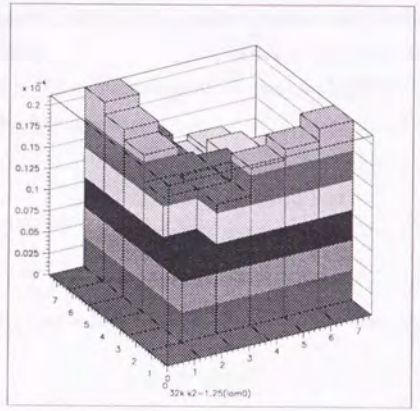

Figure 18b: The correlation $\rho(x, y)$ of the conformal mode between nearest-neighbor vertices for $\lambda = 0$, $\kappa_2 = 1.25$ with $N_4 = 32000$.

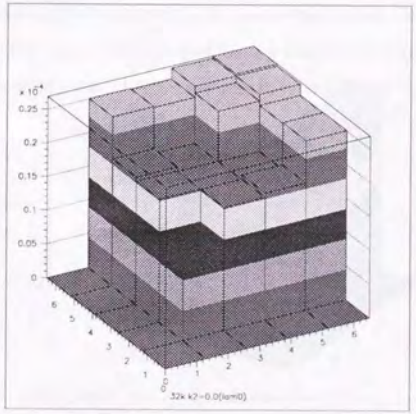

Figure 18c: The correlation $\rho(x, y)$ of the conformal mode between nearest-neighbor vertices for $\lambda = 0$, $\kappa_2 = 0.0$ with $N_4 = 32000$.

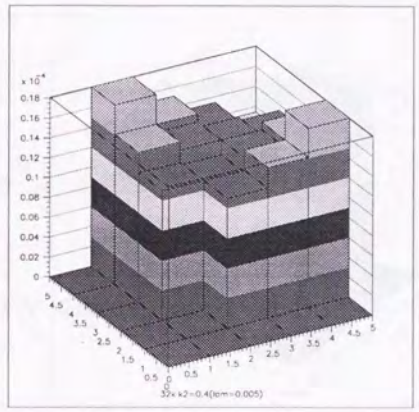

Figure 19a: The correlation $\rho(x, y)$ of the conformal mode between nearest-neighbor vertices for $\lambda = 0.005$, $\kappa_2 = 0.4$ with $N_4 = 32000$.

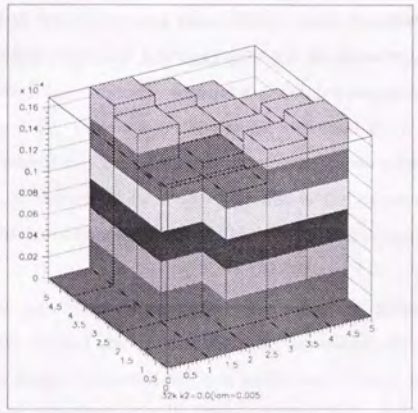

Figure 19b: The correlation $\rho(x, y)$ of the conformal mode between nearest-neighbor vertices for $\lambda = 0.005$, $\kappa_2 = 0.0$ with $N_4 = 32000$.

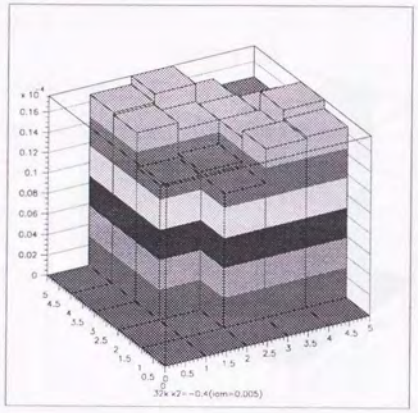

Figure 19c: The correlation $\rho(x,y)$ of the conformal mode between nearest–neighbor vertices for $\lambda = 0.005$, $\kappa_2 = -0.4$ with $N_4 = 32000$.

We see a clear anti–correlation when the system is in the branched polymer phase. In the vertex order concentration phase, on the other hand, the anti–correlation is not clearly seen. These results support the idea that the branched–polymer structure may be related to the conformal mode instability.

Chapter 4

Summary and discussion

Let us summarize the present status of numerical approach to the dynamics of quantum gravity. On Regge calculus, we reported our results in two dimensions that show a clear agreement of the loop–length distribution for the baby loops with the one obtained analytically in dynamical triangulation, when scale–invariant measure is adopted in the link–length integration. This is quite surprising considering the fact that Regge calculus does not have any grounds of restoring general covariance.

We have identified the "cutoff" with the average area of a triangle and this seems to work quite well, since we get the same universal loop–length distribution for the baby loop without any rescaling when we change the system size. If we admit that our definition of the cutoff in Regge calculus is the correct one, the negative conclusion extracted from the measurement of the string susceptibility cannot be relied upon.

We also have to consider whether the scale–invariant measure is essential or not. First of all, we remind the reader that any manifold can be arbitrarily well approximated with Regge lattice if we use sufficiently many triangles. We can, therefore, restore general covariance in Regge calculus in principle, if we introduce infinitely many parameters and fine–tune them. One may be tempted to think that our results suggest that actually we have only to impose the scale invariance to the

system. Things are not so simple, however.

When we adopt scale–invariant measure, the fluctuation of the area of each triangle is very large. This large fluctuation is certainly necessary to reproduce the fractal structure which is observed in dynamical triangulation. At the same time, we may have to worry that infinitely large triangles as well as infinitely small triangles appear in the configuration when we increase the number of triangles. This problem may be cured dynamically, since the distribution of the area of triangles may not be scale–invariant. If this is the case, the necessity of the scale–invariance of the system at the tree level becomes quite obscure. In any case, these matters should be settled in order to establish the validity of Regge calculus in studying quantum gravity.

As for the dynamical triangulation, we can rely on it as a proper regularization of quantum gravity. If we can obtain a sensible continuum limit, then we may expect to have the general covariance. We pointed out that there is a considerable freedom in the choice of the lattice action and we should not be restricted to the simplest action when we search for a non–trivial fixed point. Thus we may still have a hope also in three dimensions, where the phase transition is found to be first order for the simplest action.

In four dimensions, there is a second order phase transition. However deep in either phase, the configuration seems to have some trouble. In the weak–coupling region, the pinched structure dominates and the Haussdorff dimension is quite low. The situation might be called "branched–polymer". In the strong coupling region, on the other hand, there is a vertex with very large order. We have to clarify whether these unwanted properties of the manifold is cured at the critical point, where we hope to take the continuum limit.

We add an action which suppresses a vertex with very large order and have found that the system is always in the branched–polymer phase. From this study, we can obtain a picture of the phase transition that it is caused by the severe competition among the baby universes trying to be the dominant one. We also observed a clear anti–correlation of the conformal mode between nearest–neighbor

vertices. This suggests that the branched–polymer structure might be regarded as a manifestation of the conformal mode instability known in the continuum theory. We hope to confirm this suggestion by studying the system with an additional local action which controls the conformal–mode instability. We also think that we have to study more on three dimensions and clarify the difference from four dimensions in more detail. We should try some local actions and see if the order of the phase transition changes.

Although we cannot make any definite conclusion at present as to the continuum limit of higher–dimensional quantum gravity, we feel that the characters of the system have been revealed little by little. We hope such an effort to get qualitative information will eventually lead to the observation of a scaling behavior and the continuum physics in near future.

Acknowledgment

I would like to thank H. Kawai and T. Yukawa for stimulating discussion. I am also grateful to T. Aida, T. Izubuchi, T. Hotta, Y. Kitazawa, M. Oshikawa, A. Tsuchiya and N. Tsuda for fruitful collaboration. It is my pleasure to acknowledge K. Igi, K. Fujikawa, T. Eguchi, K. Ogawa, S. Iso, A. Yamada and all other members of particle physics group for continuous encouragement and for kind advice.

Bibliography

[1] A.M. Polyakov, Mod. Phys. Lett. **A2** (1987) 893.
V.G. Knizhnik, A.M. Polyakov and A.B. Zamolodchikov, Mod. Phys. Lett. **A3** (1988) 819.

[2] F. David, Mod. Phys. Lett. **A3** (1988) 1651.
J. Distler and H. Kawai, Nucl. Phys. **B321** (1989) 504.

[3] E. Brézin, C. Itzykson, G. Parisi and J.-B. Zuber, Commun. Math. Phys. **59** (1978) 35.
F. David, Nucl. Phys. **B257** (1985) 45.
V.A. Kazakov, Phys. Lett. **150B** (1985) 282.
D.V. Boulatov, V.A. Kazakov, I.K. Kostov and A.A. Migdal, Nucl. Phys. **B275** (1986) 641.
J. Ambjørn, B. Durhuus and J. Fröhlich, Nucl. Phys. **B257** (1985) 433.

[4] M. Goulian and M. Li, Phys. Rev. Lett. **66** (1991) 2051.
Y. Kitazawa, Phys. Lett. **B265** (1991) 262.
P. Di Francesco and D. Kutasov, Phys. Lett. **B261** (1991) 385.
Vl. S. Dotsenko, Mod. Phys. Lett. **A6** (1991) 3601.
K.-J. Hamada, preprint YITP/U-93-28, to appear in Nucl. Phys. **B**, preprint YITP/U-93-34.

[5] M. Creutz, Phys. Rev. D21 (1980) 2308, Phys. Rev. Let. 45 (1980) 313, Phys. Rev. D26 (1982) 2166.

[6] K. G. Wilson, Phys. Rev. **D10** (1974) 2445.

[7] K. G. Wilson and J. Kogut, Phys. Rep. **12** (1974) 75, and references therein.

[8] J. Nishimura, N. Tsuda and T. Yukawa, Prog. Theor. Phys. (Suppl.) **114** (1993) 19.
R. L. Renken, hep-lat/9405007, April 1994.
D. A. Johnston, J. P. Kownacki and A. Krzywicki, LPTHE-ORSAY-94-70, hep-lat/9407018, July 1994.

[9] T. Regge, Nuovo Cimento **19** (1961) 558.

[10] H.W. Hamber, Les Houches, Session XLIII (1984), K. Osterwalder and R. Stora, eds. and references therein.

[11] M. Gross and H.W. Hamber, Nucl. Phys. **B364** (1991) 703.

[12] W. Bock and J.C. Vink, UCSD/PTH 94-08, hep-lat/9406018, June 1994.

[13] C. Holm and W. Janke, FUB-HEP 06/94, hep-lat/9406020, June 1994.

[14] J. Nishimura and M. Oshikawa, Phys. Lett. **B338** (1994) 187.

[15] H. Kawai, N. Kawamoto, T. Mogami and Y. Watabiki, Phys. Lett. **B306** (1993) 19.

[16] For numerical extraction of the string susceptibility in dynamical triangulation, see : J. Ambjørn, S. Jain and G. Thorleifsson, Phys. Lett. **B307** (1993) 34.

[17] H. Kawai, private communication.

[18] N. Tsuda and T. Yukawa, Phys. Lett. **B305** (1993) 223.

[19] G. 't Hooft and M. Veltman, Ann. Inst. Henri Poincare **20** (1974) 69.

[20] G. Gibbons, S. Hawking and M. Perry, Nucl. Phys. **B138** (1978) 141; S. W. Hawking, in General Relativity, an Einstein Centenary Survey, eds. S.W. Hawking and W. Israel (Cambridge University Press, 1979).

[21] S. Weinberg, in General Relativity, an Einstein Centenary Survey, eds. S.W. Hawking and W. Israel (Cambridge University Press, 1979).
R. Gastmans, R. Kallosh and C. Truffin, Nucl. Phys. **B133** (1978) 417.
S.M. Christensen and M.J. Duff, Phys. Lett. **B79** (1978) 213.

[22] H. Kawai and M. Ninomiya, Nucl. Phys. **B336** (1990)115.

[23] H. Kawai, Y. Kitazawa and M. Ninomiya, Nucl. Phys. **B393**(1993) 280.

[24] H. Kawai, Y. Kitazawa and M. Ninomiya, Nucl. Phys. **B404** (1993) 684.

[25] J. Nishimura, S. Tamura and A. Tsuchiya, UT-664,ICRR-Report-308-94-1,UT-Komaba/94-2, to appear in Int. J. Mod. Phys. A.

[26] J. Nishimura, S. Tamura and A. Tsuchiya, KEK-TH-394,ICRR-Report-318-94-13,UT-Komaba/94-11, to appear in Mod. Phys. Lett. A.

[27] S.-I. Kojima, N. Sakai and Y. Tanii, TIT preprint, TIT-HEP-238, November 1993, hep-th 9311045.
Y. Tanii, S.-I. Kojima and N. Sakai, Phys. Lett. **B322** (1994) 59.

[28] T. Aida, Y. Kitazawa, H. Kawai and M. Ninomiya, Nucl. Phys. **B427** (1994) 158.

[29] T. Aida, Y. Kitazawa, J. Nishimura and A. Tsuchiya, TIT-HEP-275, KEK-TH-423, UT-Komaba/94/22, Dec. 1994.

[30] M. Gross and S. Varsted, Nucl. Phys. **B378** (1992) 367.

[31] J. W. Alexander, Ann. Math **31** (1930) 292.

[32] J. Ambjørn and S. Varsted, Phys. Lett. **B266** (1991) 285, Nucl. Phys. **B373** (1992) 557.

[33] J. Ambjørn, D. V. Boulatov, A. Krzywicki and S. Varsted, Phys. Lett. **B276** (1992) 432.
J. Ambjørn and S. Varsted, Nucl. Phys. **B373** (1992) 557.

[34] C. F. Baillie, Phys. Rev. **D46** (1992) 2480.
R. L. Renken, S. M. Catterall and J. B. Kogut, Nucl. Phys. **B389** (1993) 601.
J. Ambjørn, Z. Burda, J. Jurkiewicz and C. F. Kristjansen, Phys. Lett. **B297** (1992) 253.

[35] J. Ambjørn and J. Jurkiewicz, Phys. Lett. **B278** (1992) 42
M. E. Agishtein and A. A. Migdal, Mod. Phys. Lett. **A7** (1992) 1039; Nucl. Phys. **B385** (1992) 395.
S. Varsted, Nucl. Phys. **B412** (1994) 406.

[36] B. Brügmann, Phys. Rev. **D47** (1993) 330.
B. Brügmann and E. Marinari, Phys. Rev. Lett. **70** (1993) 1908.

[37] S. Catterall, J. Kogut and R. Renken, CERN-TH.7197/94, ILL-(TH)-94-07, hep-lat/9403019, Mar. 1994.
J. Ambjørn and J. Jurkiewicz, preprint NBI-HE-94-29, hep-lat/9405010, May 1994.
B. V. de Bakker and J. Smit, ITFA-9-14, hep-lat/9405013, May 1994.
B. Brügmann and E. Marinari, MPI-PhT/94-72, hep-th/9411060, Nov. 1994.

[38] S. Jain and S. D. Mathur, Phys. Lett. **286** (1992) 239.
J. Ambjørn, S. Jain, J. Jurkiewicz and C. F. Kristjansen, Phys. Lett. **B305** (1993) 208.

[39] T. Hotta, T. Izubuchi and J. Nishimura, in preparation.